AEDC-TR-77-69

cy. 2

ELECTRICAL AND THERMAL CONDUCTIVITY AND RADIATION POWER OF AIR MEASURED AT 1-30 ATM AND 6500-11500°K

GEORGIA INSTITUTE OF TECHNOLOGY
ATLANTA, GEORGIA 30332

June 1977

Final Report for Period June 1974 - September 1975

Approved for public release; distribution unlimited.

Prepared for

DIRECTORATE OF TECHNOLOGY
ARNOLD ENGINEERING DEVELOPMENT CENTER
AIR FORCE SYSTEMS COMMAND
ARNOLD AIR FORCE STATION, TENNESSEE 37389

NOTICES

When U. S. Government drawings specifications, or other data are used for any purpose other than a definitely related Government procurement operation, the Government thereby incurs no responsibility nor any obligation whatsoever, and the fact that the Government may have formulated, furnished, or in any way supplied the said drawings, specifications, or other data, is not to be regarded by implication or otherwise, or in any manner licensing the holder or any other person or corporation, or conveying any rights or permission to manufacture, use, or sell any patented invention that may in any way be related thereto.

Qualified users may obtain copies of this report from the Defense Documentation Center.

References to named commercial products in this report are not to be considered in any sense as an endorsement of the product by the United States Air Force or the Government.

This final report was submitted by Georgia Institute of Technology, Atlanta, Georgia 30332, under contract F40600-76-C-0004, with the Arnold Engineering Development Center, Arnold Air Force Station, Tennessee 37389. Dr. M. L. Laster was the AEDC technical monitor.

This report has been reviewed by the Information Office (OI) and is releasable to the National Technical Information Service (NTIS). At NTIS, it will be available to the general public, including foreign nations.

APPROVAL STATEMENT

This technical report has been reviewed and is approved for publication.

FOR THE COMMANDER

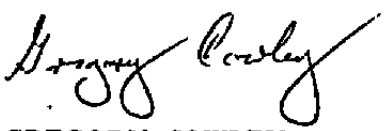

GREGORY COWLEY
Second Lieutenant, USAF
Research & Development
Division
Directorate of Technology

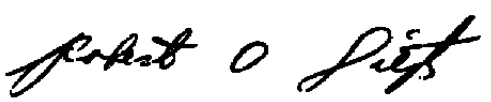

ROBERT O. DIETZ
Director of Technology

REPORT DOCUMENTATION PAGE		READ INSTRUCTIONS BEFORE COMPLETING FORM
1 REPORT NUMBER AEDC-TR-77-69	2 GOVT ACCESSION NO.	3 RECIPIENT'S CATALOG NUMBER
4 TITLE (and Subtitle) ELECTRICAL AND THERMAL CONDUCTIVITY AND RADIATION POWER OF AIR MEASURED AT 1-30 ATM AND 6500-11500°K		5 TYPE OF REPORT & PERIOD COVERED Final Report - June 1974 - September 1975 6 PERFORMING ORG. REPORT NUMBER
7 AUTHOR(s) A. V. Larson and J. R. Williams		8 CONTRACT OR GRANT NUMBER(s) F40600-76-C-0004 F40600-74-C-0007
9 PERFORMING ORGANIZATION NAME AND ADDRESS Georgia Institute of Technology Atlanta, Georgia 30332		10 PROGRAM ELEMENT, PROJECT, TASK AREA & WORK UNIT NUMBERS Program Element 65807F
11 CONTROLLING OFFICE NAME AND ADDRESS Arnold Engineering Development Center (DYFS) Air Force Systems Command Arnold Air Force Station, Tennessee 37389		12 REPORT DATE June 1977 13 NUMBER OF PAGES 51
14 MONITORING AGENCY NAME & ADDRESS(if different from Controlling Office)		15 SECURITY CLASS. (of this report) UNCLASSIFIED 15a DECLASSIFICATION DOWNGRADING SCHEDULE N/A

16 DISTRIBUTION STATEMENT (of this Report)

Approved for public release; distribution unlimited.

17. DISTRIBUTION STATEMENT (of the abstract entered in Block 20, if different from Report)

18 SUPPLEMENTARY NOTES

Available in DDC

19 KEY WORDS (Continue on reverse side if necessary and identify by block number)

air
plasmas(physics)
electrical conductivity
thermal conductivity
radiation
arc heaters

20 ABSTRACT (Continue on reverse side if necessary and identify by block number)

Experimental results are reported on the electrical and thermal conductivities and the radiative properties of air plasma at pressures of 1, 6 and 30 atm. in the temperature range 6,500°K to 11,500°K. A wall-stabilized steady cascade arc was used to provide a cylindrically symmetric column of air plasma. The electrodes were bathed in argon. The electrically floating wall plates were used to determine the electric field strength in the column. Side-on optical measurements of the lateral intensity profile using the

DD FORM 1 JAN 73 1473 EDITION OF 1 NOV 65 IS OBSOLETE

20. ABSTRACT (Continued)

oxygen 844. 6 nm line and the nearby continuum permitted the deduction of the radial temperature profile using the Abel Inversion. Total radiation per unit arc length for wavelengths transmitted through a quartz window was measured by a thermopile. Temperature dependent trial functions of electrical conductivity and radiation strength per unit volume were optimized by computer to fit the experimental data. Thermal conductivity was then obtained from the energy balance. The experimental results agree well with the existing experiments and theories at 1 atm. At the higher pressures, the experiments are original and compare favorably to theory.

AFSC
Arnold AFB Tenn

PREFACE

The experimental work reported herein was conducted at the Georgia Institute of Technology, Atlanta, Georgia, and was supported in part by the Arnold Engineering Development Center, Air Force Systems Command, under Contract F40600-74-C-0007, during the period June 1974 to September 1975. Additional analytical work was done thereafter in part under Contract F40600-76-C-0004. The AEDC technical monitor for these contracts was Dr. M. L. Laster. The Program Element was 65807F.

The authors are indebted to Dr. S. D. Thompson for the Abel inversion program and the initial spectroscopic investigations; Mr. Jeff A. Madill, B.S.E.S.M. for most of the computer programming and data management and for able assistance in the laboratory; Mr. J. P. Tinkham, Research Specialist, for the experimental set-ups and care of the laboratory; Mr. Craig Wynn, Mr. Dan Reed, Mr. Bill Newberry, students who assisted in data taking and management; and the personnel at AEDC who maintained a close interest in this work, Dr. M. Laster and Maj. U. L. Barnwell, and Dr. W. K. McGregor and Mr. Joe Sprouse of ARO, Inc., AEDC Division, operating contractor of AEDC.

The reproducibles used in the reproduction of this report were supplied by the authors.

CONTENTS

LIST OF FIGURES AND TABLES

FIGURE

TABLE

INTRODUCTION

Air occurs at high pressure and high temperature in several phenomena which are important to the Air Force. One of these, reentry, is being studied at the Arnold Engineering Development Center with air streams heated by electric arcs. Development of high power, high pressure arcs is being pursued also to advance the state of the arc heater facilities. Experimental knowledge of the electrical and thermal conductivities and the radiation source strength is needed for air at pressures up to 250 atm. and temperatures near 10,000°K. Research has been done at the Georgia Institute of Technology using wall-stabilized cascade arcs for the determination of those properties. Data is reported here for pressures up to 30 atm., the goal of the initial effort.

The work was started because theoretical predictions of the properties of air at high pressure and temperature lacked verification. Dissociation, ionization, and non-ideality must be included in the calculations and give rise to uncertainties since some of the fundamental particle interaction probabilities are poorly known. It is a common practice to "tune" the theory by choosing multiplicative constants for the collision integrals in such a way that the theory agrees with the best available experimental data. This method was used recently by Nicolet, et. al., in a most thorough theoretical and design study for a high-pressure, high-enthalpy constricted arc heater (Ref. 1). At that time, the tuning was done at 1 atm. since no experimental data existed at higher pressures. The extrapolation of the tuned theory to high pressures is subject to additional error due to the changing composition. For example, Nicolet points out that the e - N_2 collision is dominant at 100 atm., 8000°K but is far less important at 1 atm., 8000°K.

Thus experiments are needed at high pressure both for the original data which can be generated and for the verification or stimulation of theoretical calculations. Andreev and Gavrilova (Ref. 2) report some initial data on the electrical conductivity in pulsed air arcs at $95 \leq p \leq 150$ atm. and $13{,}400 \leq T \leq 18{,}000$°K. Prior to their work, experimental knowledge of air plasmas was limited to atmospheric pressure. Comparisons of calculations and experiments on the electrical conductivity of air at 1 atm. have been given over the temperature range 4,000 to 16,000°K (Ref. 3) and 8,000 to 12,500°K (Ref. 4). Similar comparisons for the thermal conductivity of air at 1 atm. exist in the interval 1,000 to 17,000°K (Ref. 3). A summary of available knowledge for the total radiant power of air plasma at 1 atm. between 9,000 and 14,000°K appears in Ref. 4.

There has been a steadily growing capability in the use of confined arcs for the measurement of the properties of plasmas. The development more than a decade ago of the wall-stabilized cascade arc (Ref. 5) has allowed the arc to be studied scientifically at high power levels, and thus high gas temperatures. Extensive arc research programs have been described by groups at Harvard (Emmons, Ref. 6), USSR Institute for High Temperatures (Asinovsky, Ref. 3), AVCO Corporation (Morris, Ref. 7), National Bureau of Standards (Venable, Ref. 8), Munich's Electrophysical Institute (Maecker, Ref. 9), the Aerospace Research Laboratories, Wright-Patterson AF Base (Bauder, Ref. 9 and Schreiber, Ref. 4), and others. Some related calculational techniques have been discussed by Devoto (Ref. 10).

In order to measure the properties of high pressure plasmas, a sophisticated high pressure arc plasma laboratory was developed in the late sixties by the Air Force at the Thermomechanics Research Laboratory at the Wright Patterson Air Force Base. In 1972 this laboratory was transferred to the Georgia Institute of Technology. In this facility, the cascade arc appartus can be assembled in a pressure vessel with optical viewing ports, so that the arc heated column can be studied at high pressures by means of electrical, optical, and thermal measurements. The laboratory capabilities extend to 1000 atm. pressure and to arc temperatures of 30,000°K.

The experiments reported herein were conducted at pressures of 1, 6, and 30 atm. at temperatures between 6,500°K and 11,500°K approximately. Spectroscopic measurements were used to deduce the temperature profile in the arc. Then the electrical conductivity was determined as a function of temperature. The radiation from the arc was measured and the thermal conductivity was calculated from the energy balance equation. The total radiation and the thermal conductivity measurements are as yet incomplete in that the radiation spectrum was limited by fused silica windows. Nevertheless agreement with theory is reported at the lower pressures for the thermal conductivity when it is calculated from the energy balance for an optically thin arc.

THEORY

It is possible under certain circumstances to operate an arc column which in its central part has cylindrical symmetry and no axial gradients except for a constant voltage gradient. The energy balance per unit volume for an optically thin plasma in local thermodynamic equilibrium becomes

$$\sigma E^2 - u + \frac{1}{r}\frac{d}{dr}\left(rk\frac{dT}{dr}\right) = 0 \qquad (1)$$

where r is the radius of a general observation point,

σ is the electrical conductivity

E is the electric field strength

u is the radiation source strength

k is the thermal conductivity and

T is the equilibrium temperature at r.

The first term is the electrical power input, the next is the radiative power lost and the last is the conduction term. Convection is usually unimportant.

The functions to be determined are $\sigma(T)$, $u(T)$, and $k(T)$. If the temperature is highly uniform across most of the arc, one can obtain direct information on $\sigma(T)$, and $u(T)$. Usually however, $T = T(r)$ which necessitates deducing the properties from the integral quantities given below.

The observables are the arc electric field and current, E(I), the total radiation per unity arc length, P_r, and the chordal radiation intensity. From basic definitions,

$$I = 2\pi \int_0^R \sigma E r \, dr = 2\pi E \int_0^R \sigma r \, dr \tag{2}$$

$$P_r = 2\pi \int_0^R ur \, dr \tag{3}$$

where the approximation $E \neq E(r)$ is assumed to be valid in the experimental apparatus. R is the arc radius.

Several techniques (Ref. 6, 10) exist for the deduction of $\sigma(T)$ if the radial temperature profile $T_i(r)$ has been determined for several arc conditions $E_i(I_i)$. The same techniques are applicable in obtaining $u(T)$ if P_{ri} has also been measured. For example, a trial function with arbitrary constants may be assumed for $\sigma(T)$. Then for each arc condition, $T_i(r)$ is used to obtain $\sigma_i(r)$. The integral in equation (2) is evaluated and compared to the experimental values of I_i/E_i. Then the arbitrary constants in $\sigma(T)$ are adjusted until a best fit is found for a series of arcs $E_i(I_i)$ at a given pressure.

It is possible to determine $T_i(r)$ in a stable, cylindrically symmetric, optically thin arc, which is in thermodynamic equilibrium. For example, one can use the total radiation of the particular atomic line transition. The chordal intensity, I(y), of this radiation which is viewed along a chord of the arc is measured as a function of the distance, y, of the chord from the arc center. Because of the cylindrical symmetry, I(y) can be converted by means of the Abel integral inversion, to a local volume emission coefficient, $\varepsilon(r)$. From knowledge of atomic theory and atomic parameters measured in other experiments, one can correlate the emission coefficient with the local temperature $\varepsilon(T)$. Then by comparison, one deduces T(r). The technique is explained by Griem (Ref. 11).

In the experimental program, then, T(r) is deduced from spectroscopic measurements. The $T_i(r)$, P_{ri}, I_i, E_i, for a set of arc conditions (i) allow a deduction of $\sigma(T)$ and $u(T)$, using equations (2) and (3). Finally $k(T)$ can be calculated from equation (1) since it is the only unknown.

The deduction of $u(T)$ and $k(T)$ is much more complicated if the arc reabsorbs some of its own radiation. Morris (Ref. 7) gives a good example of the radiation transport calculations which must be done for such an arc.

APPARATUS

CASCADE ARC

An unrestrained arc between two electrodes can be very unstable which makes it of little use for the determination of plasma properties. One method of stabilizing an arc is to physically constrain it in a channel, such as illustrated in Figure 1. This device is called a cascade arc; here the arc is confined in a circular channel in the center of a stack of copper water-cooled cascade plates, which are insulated from each other and at floating potential. A properly designed cascade arc will operate stably over a certain range of currents and pressures.

The insulators between the plates also serve as gas seals so that the purity of the test gas in the central test section may be maintained. Air is admitted to the test section through ports between selected plates while the electrodes are bathed in argon by other ports. The interfaces between the gases are controlled in part by breather passages between plates near the electrodes. In the present work air was admitted only where shown. The tubes near the anode were replaced by gas seals.

The wall-stabilized arc can usually be examined spectroscopically by providing side-on observation ports between two adjacent central plates. Such measurements are necessary to verify the purity of the test gas and to measure the temperature profile and the radiation characteristics.

Figure 2 illustrates the construction and operation of a cascade arc. On the left is shown an exploded view of a single copper cascade plate. The cascade plates are constructed of high purity oxygen-free copper. The lower plate is engraved with cooling channels and the upper plate is diffusion bonded to the lower with silver. The total thickness of the completed cascade plate (lower figure) is 2mm, and the central bore is either 3 or 4mm for the present studies.

These cascade plates are separated by 0.3mm thick silicone rubber washers. The holes at the corners of the plate form cooling channels. Cooling water enters through two of these holes in opposite corners, and flows out through the other two holes. The high flow velocity along the curved section of the cooling channel, adjacent to the central bore, results in a very high convective heat transfer coefficient; bubbles of water vapor produced by nucleate boiling are swept away as fast as they form.

The cooling water exiting the cascade is maintained at a pressure equal to that of the gas in the pressure vessel. Pressure equalization at all times is maintained by an accumulator, as illustrated in Figure 2; a diaphragm in the accumulator prevents absorption of the gas by cooling water at high pressure.

Only one gas system is shown Figure 2: It supplies the chamber pressure either directly or through a compressor if pressures greater than bottle pressure are desired. Not shown are the supply systems for the test gas (air) or the electrode blanket (argon). Their pressures are referenced to the chamber pressure by differential transducers and their flows are separately

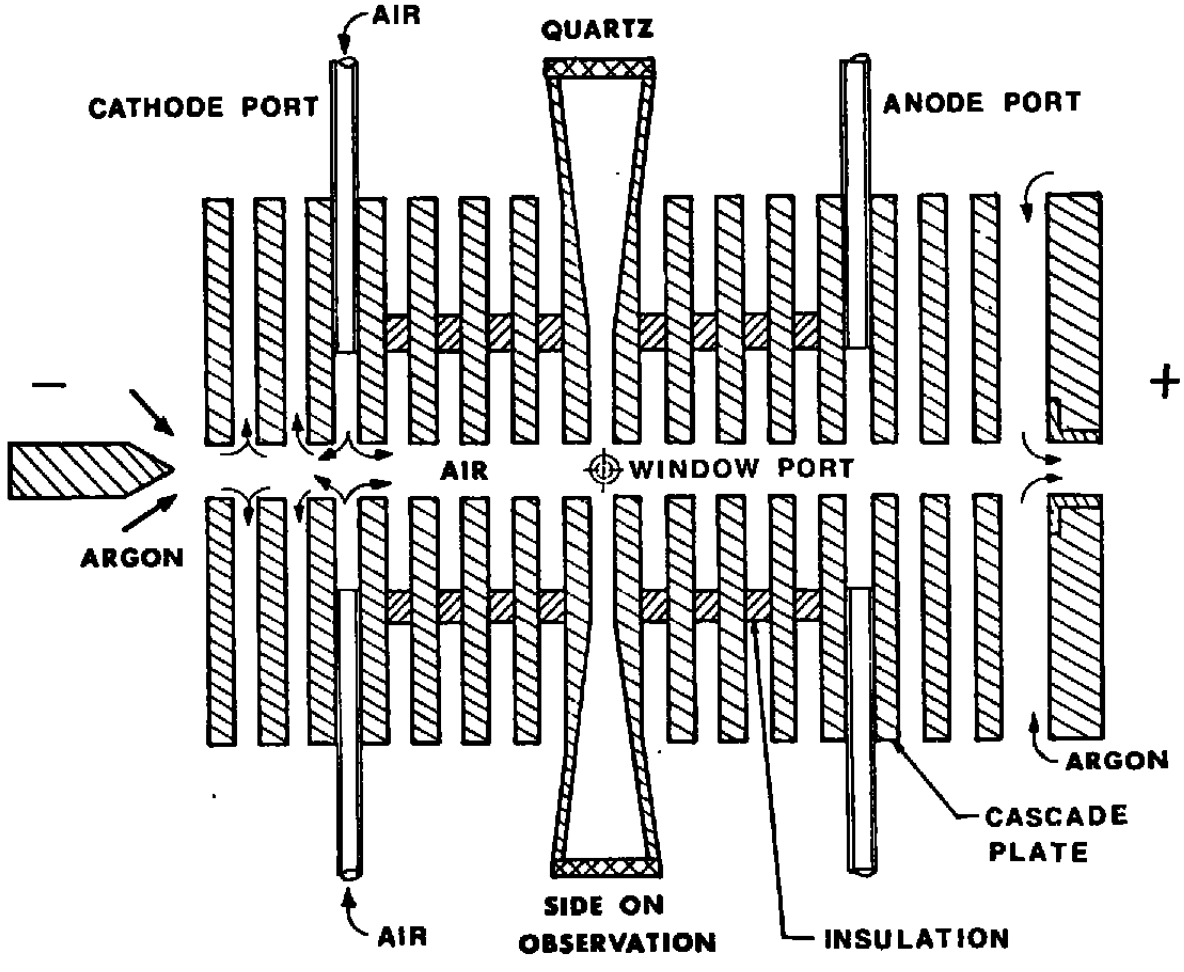

Figure 1. Schematic Diagram of Arc Apparatus.

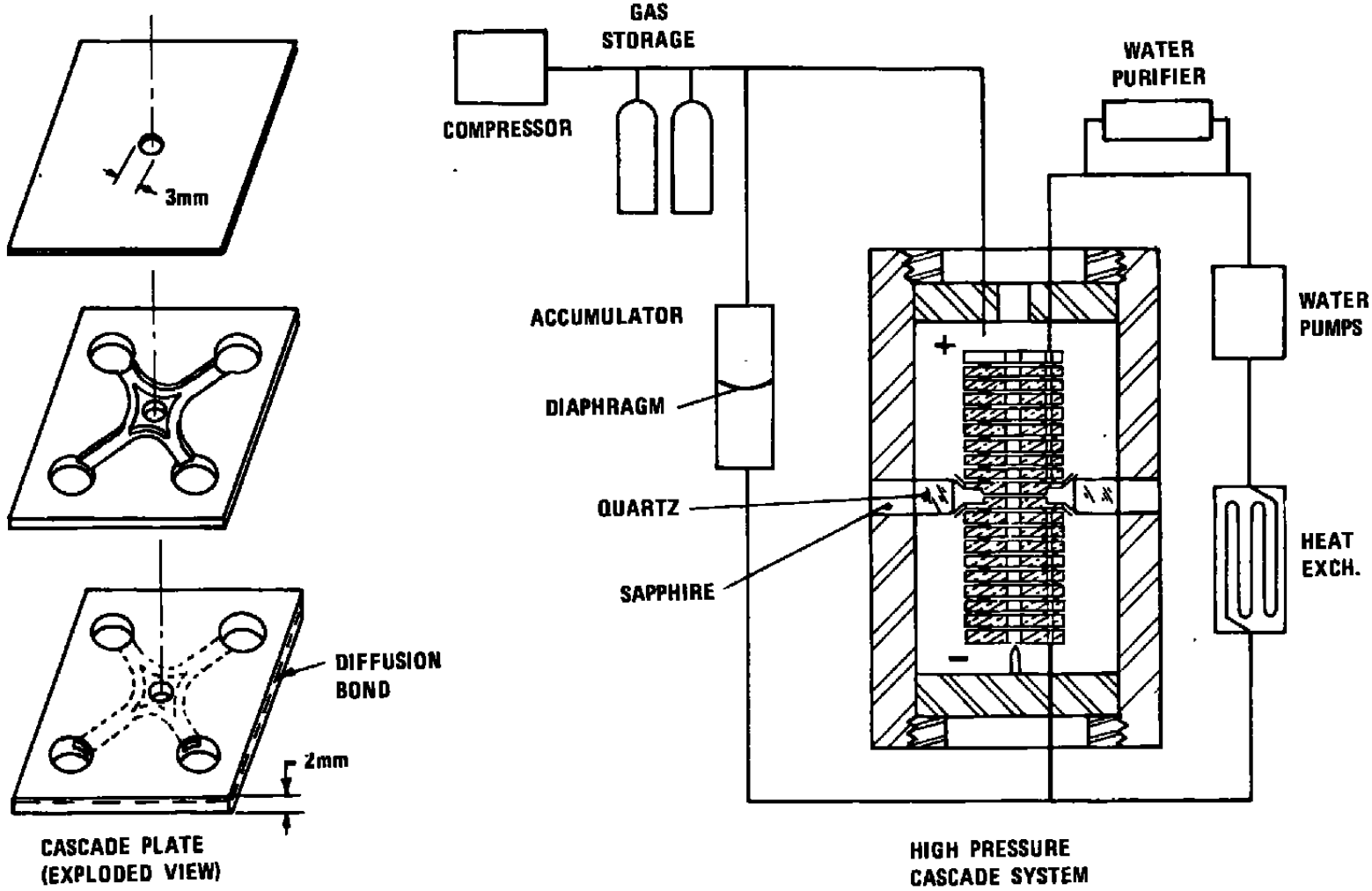

Figure 2. Cascade Plate and Arc Assembly Schematic Showing Gas and Cooling Water Flows

controlled by needle valves.

The other auxiliary equipment shown in Figure 2 have been previously described (Ref.12).

Figure 3 shows the cascade arc in various stages of assembly. Four guide tubes are inserted into the cooling channels to help align the plates during assembly; they are removed when assembly is complete. The cooling water flows into the copper manifold, through the cooling channels in each cascade plate, and out through the copper manifolds. Electrical leads connected to each plate (left side of lower right photo) allow the voltage reached by each plate to be monitored while the arc is operating so that the electric field strength in the arc can be determined. The window port, for viewing the test section in the center of the cascade, is made up using two specially engraved plates as shown in the upper right photograph. Grooves are cut into the plate on opposite sides of the arc to permit less-obstructed viewing of the arc and are blackened electrochemically. The lower left photograph shows the resulting window port opening. This port is covered by a quartz window to provide the gas seal and a shroud (lower right) to reduce convection currents around the window. Breather ports are located near the anode and cathode to allow the test gas and argon to exit.

The gases are injected into the cascade through small gas ports inserted between the cascade plates. The tubes which feed the test section and bathe the anode stick out prominently from the cascade in the lower left photo, and the gas flow tubes connecting them are shown in the lower right.

Figure 4 shows front and side views of the cascade arc assembly. The voltage probes connected to the cascade plates are prominent in the side view. The arc is visible from the front at five locations; through the window port at the center of the cascade, between three plates at the anode, and between three plates at the cathode. Observation of the arc at the cathode and anode is important for observing arc stability and determining argon purity at these locations.

Two gas flow manifolds are shown at the bottom of the front view. One-quarter inch copper tubing is connected to four small flexible tubes leading to the gas ports entering the four sides of the cascade. The gas exits the arc into a copper water-cooled exhaust chamber located above the arc.

The water-cooled thoriated tungsten cathode is typically a sharpened cone 6mm in diameter at the base and is located on the axis of the assembly below the arc. The anode is a 5mm thick copper cascade plate with a tungsten insert in the central bore, and is located at the top of the cascade. Between 10 and 16 cascade plates are used in the assembly, depending on the bore diameter and the characteristics of the test gas.

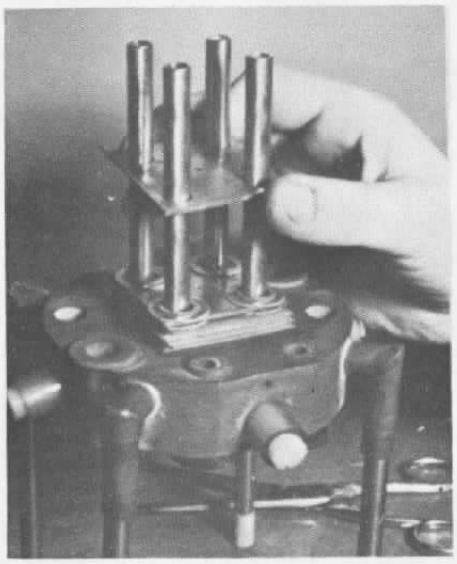

Breather Ports

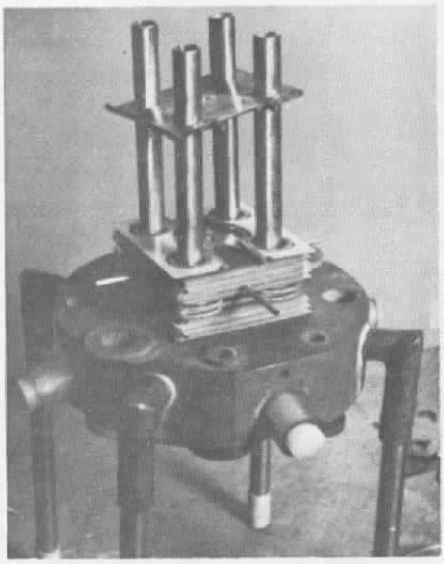

Window Ports

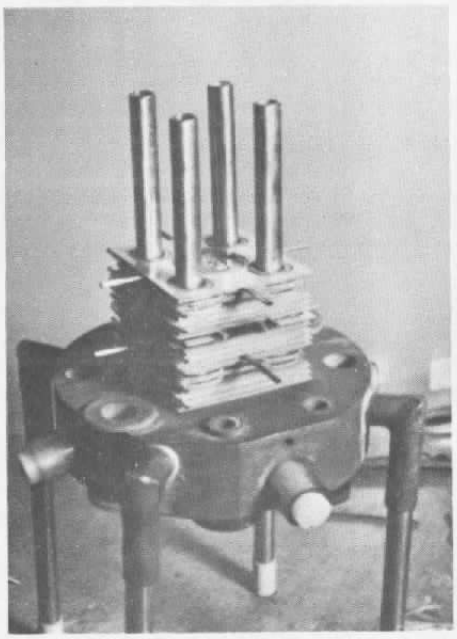

Anode Argon Flow Section

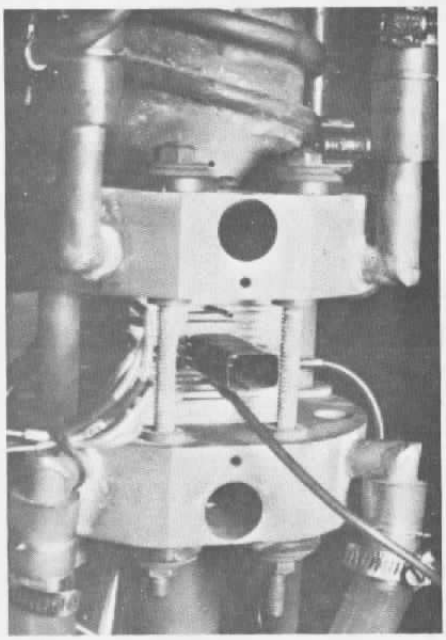

Completed Cascade

Figure 3. Assembly of Cascade Arc

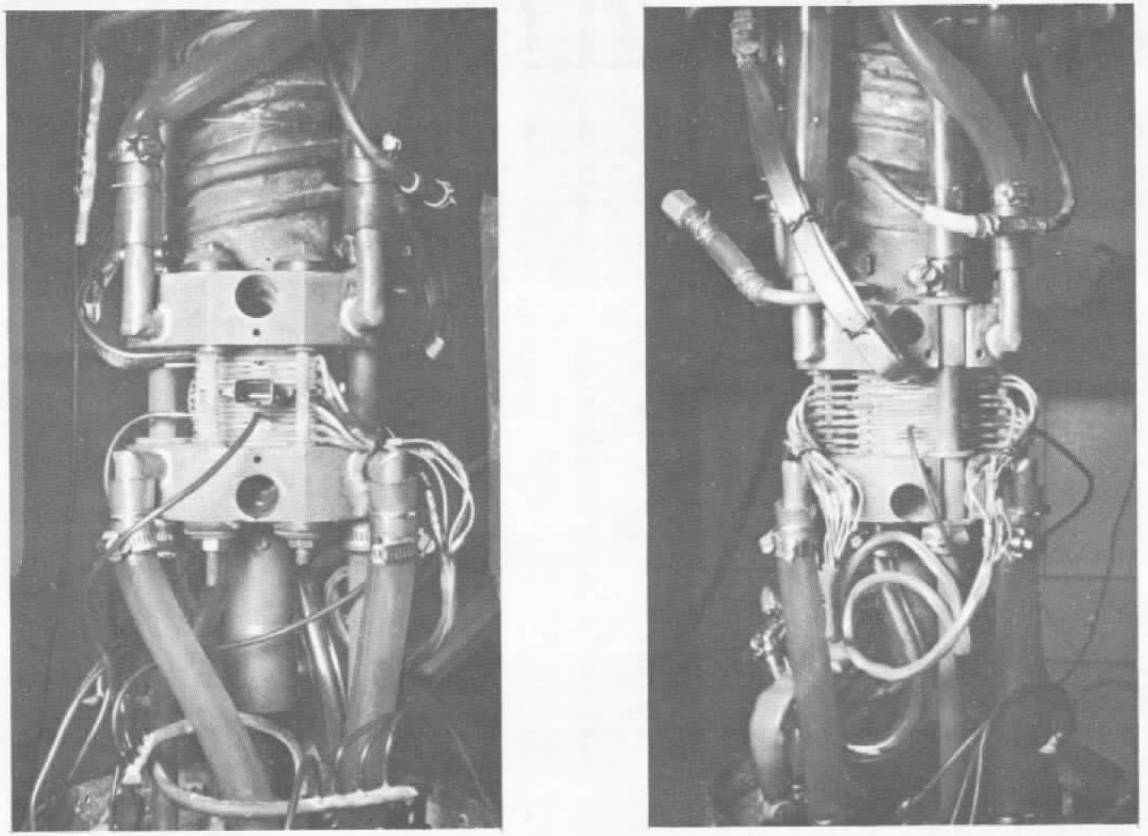

Figure 4. Complete Cascade Arc Assembly (Front View - left, Side View - right)

HIGH PRESSURE APPARATUS

The cascade arc assembly is operated within a high pressure vessel containing quartz or sapphire windows for viewing the arc from opposite sides, connections for the water and gas flows, and electrical connectors for powering the arc and measuring its electrical parameters. The laboratory contains four of these pressure vessels, two for operation at pressures to 200 atm, and two for operation at pressures to 1,000 atm.

Figure 5 (upper) shows one of the 200 atm vessels. Dr. Larson is examining a thermopile which is used for measurements of the total arc intensity. One of the 1,000 atm chambers is shown in the lower photo; Dr. Williams and Mr. Wynn are aligning the scanning mirror for the spectrographic measurements. The upper end plug with the cascade arc assembly attached can be removed using an overhead crane.

The pressure vessels and associated apparatus (Ref.12) are located in a section of the laboratory surrounded by a blast wall consisting of sandbags backed up by anchored walls made of large concrete blocks. All operations are done by remote control except for those with the spectrometer. Radiant energy from the arc is reflected from the scanning mirror through a slit in the concrete wall, and a magnified image of the arc is formed on the entrance slit of the spectrometer on the other side of the wall.

INSTRUMENTATION

A schematic of the instrumentation for the spectroscopic measurements is found in Figure 6, and the components are described in Table 1. The arc image was focused on the entrance slit of the spectrometer by means of the lens and a high quality front surface mirror. The arc image was swept across the spectrometer entrance at a constant rate in order to measure the lateral intensity profile. The scanning mirror was rotated about a vertical axis in its front surface by a reversible synchronous motor through a Gaertner reducer and slide. The scanning rate was determined by geometry and by measurement when the arc was replaced by rear-illuminated rods of known thickness.

The calibration of the intensity was done by turning the mirror 90° counterclockwise so that an image of a tungsten ribbon in a standard calibration lamp was focused on the spectrometer entrance. Equivalent optical paths were established for the arc and the ribbon by the use of identical window insertions. The tungsten ribbon standard lamp was part of an EG&G Model 590 Calibrated Lamp System with its calibration traceable to the National Bureau of Standards.

The arc image at the spectrometer was several millimeters wide. The entrance slits were opened to .03mm to give a fine spatial resolution. A dual exit system for the spectrometer allowed for photographic or photoelectronic measurement of the radiation in a certain wavelength band. Photographic measurements of an argon arc were used to determine the linear reciprocal dispersion which was 6.70 Angstrom/mm of the exit opening.

Viewing the arc through the left windows in Figure 6 was a thermopile (not shown) described in Table 1. A parallel slit system was mounted on the inner quartz window in order to simplify the geometry of the arc slice being observed. The combination of a slit shutter and a nanovoltmeter with a signal suppression circuit was used to subtract the background radiation which was present.

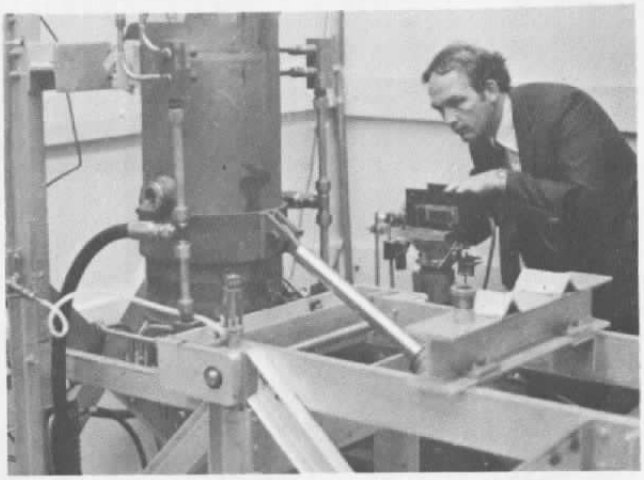

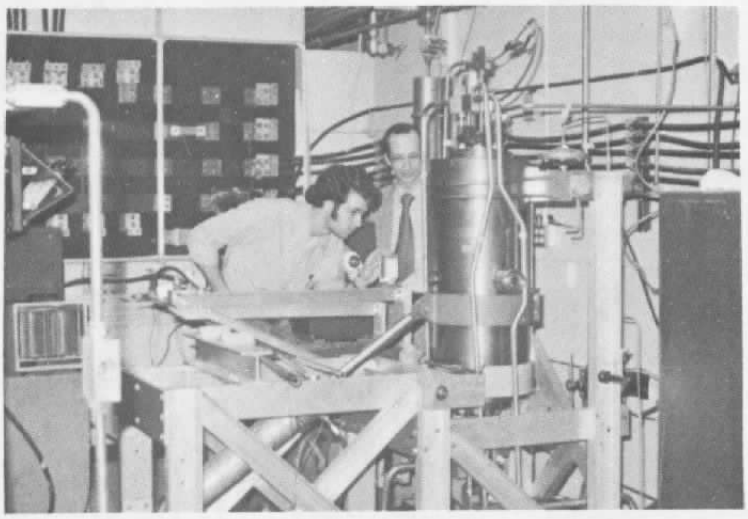

Figure 5. 200 Atm (upper) and 1000 Atm (lower) Pressure Chambers

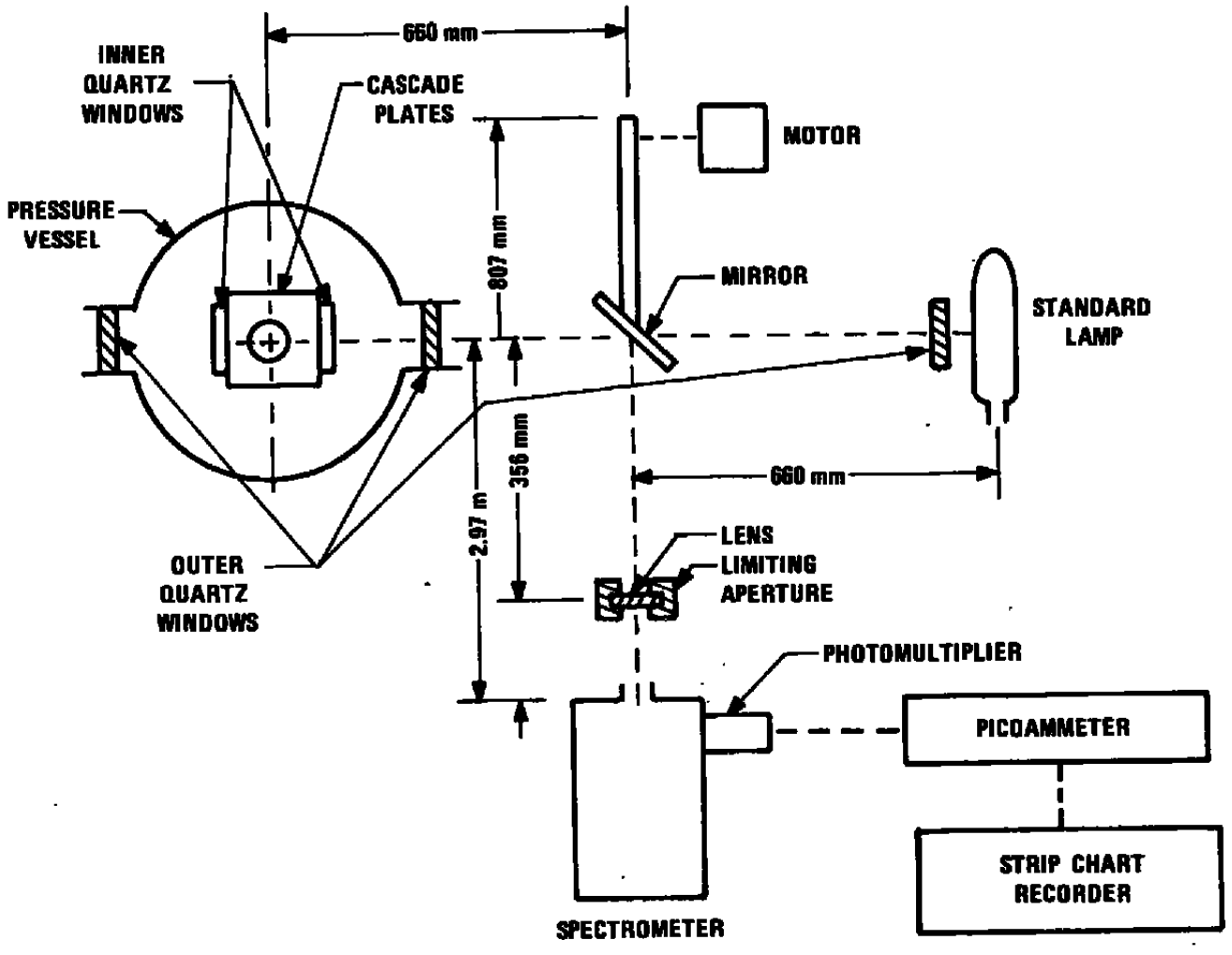

Figure 6. Schematic of Experimental Apparatus, Excluding the Thermopile

TABLE I: INSTRUMENTATION

Lens: Karl Lambrecht
Crystal-Quartz-Lithium Floride Achromatic
Objective Lens
Diameter 32mm
Focal Length 80 ± 5cm
Limiting Aperture 38mm outside, 29mm clear

Spectrometer: McPherson 2051

Photomultiplier: EMI 9658R
S-20

Picoammeter: Keithley Instruments
Model 416
Response Time ≈ .004 sec

Strip Chart Recorder: Clevite Brush
Mark 250 Recorder

X-Y Recorder: Hewlett-Packard
Model 7004A

Standard Lamp: EG & G
Model 590
Calibrated Lamp System
5920 Lamp Housing

Calibrated by Epply Laboratories, Inc.
National Bureau of Standards Reference
Standards Employed: EU 285, EU 286, EU 289

Nanovoltmeter: Keithley Instruments, Inc.
Model 148

Thermopile: Hilger-Schwarz
Type FT 19/463
Receiver Dimensions: 2x.2mm
Sensitivity: 25 μV/μW
Response Time: .01 sec
Spectral Range: 110-10000nm

Four channels of an HP3480 DVM with an HP3485A scanning unit were used to display arc current, voltage, electric field strength, and pressure. An HP5050B digital recorder printed this information during the actual scan of the arc. The arc current was measured by a precision shunt in the cathode lead. The electric field strength was measured in two ways. First, the voltage difference between two cascade plates near either end of the uniform test section was displayed on the HP3480 DVM. The field strength was calculated as the voltage difference divided by the plate separation distance. In addition, an HP7004A X-Y recorder plotted the cascade plate voltage-vs-distance from the cathode. The slope of the plot is a measure of the electric field strength. In addition, this plot was a check on arc stability and a visual verification of the lack of axial nonuniformities in the test section if the plot was linear in that region.

Optical alignment of the system was done using a 2mw red laser penetrating the exit of the spectrometer and exiting from the spectrometer entrance slits. The calibration of the tungsten ribbon lamp is measured from time to time versus another such lamp which is used only for reference purposes. The thermopile is calibrated against a blackbody operating at 1273°K. The electronic calibrations are done in a standard manner.

PRELIMINARY EXPERIMENTS

At the start of the study no work which was known to the authors had been done on air arcs at pressures above one atm. Therefore a step-by-step procedure was chosen to advance the technology of the apparatus and to check on any possible scientific problems standing in the way of success. The procedure was to establish a successful air arc at one atmosphere, to repeat some of the work in the literature (Ref. 3,4) to verify the apparatus, measurements and analysis techniques at Georgia Tech, and then to generate new results at 30 atm. At each pressure sufficient lifetime of the plate and electrode structure was necessary before the requirements for a stable, pure air, axisymmetric column free from axial gradients (except a voltage gradient) and flow effects could be checked thoroughly. Then spectroscopic data could be taken in search of data suitable for unambiguous interpretation. Fortunately none of these steps proved prohibitive to success of the program, although each has hindered the rate of progress. Comments on these matters and the preliminary experiments follow.

Setting up the apparatus and conducting the preliminary experiments are described in more detail elsewhere (Ref. 13, 14). Comments here are mostly from experience in air arcs at 6 and 30 atm.

Figure 1 illustrates schematically the approximate set-up for the early experiments at 1 atm. (Ref. 13). The only controlled gas flow was the air flow. The argon near the electrodes (if any) was supplied from the ambient chamber filling gas by natural processes. The life-time of the plate-electrode structure was 5 to 15 minutes, which was inadequate in relation to the rebuilding time of four days.

The typical life-time of the apparatus was extended by the present authors to several hours by forced control of the argon flows and by many trials involving air insertion methods, breather port location, and plate spacing. The cathode region is now sealed from the pressure chamber so that the argon flow near the cathode is controlled externally. Likewise for the region between the anode and its nearest plate. A vortex input arrangement for the argon has seemed to help in both regions. A water cooled exhaust hood is mounted just above the anode and is bled off to the outside to keep the chamber pressure constant.

The lifetime of the apparatus is affected by arc instability which can lead to shorted plates or to more rapid electrode wear. The major factor however appears to be the condition of the plates and the difficulty of achieving zero-defect in over a hundred water and gas seals under pressure.

In the present configuration, for any given day, the likelihood of acquiring good data sets is excellent at pressures below 10 atm., but is more like 50% when taking data at 30 atm. At the higher pressure, runs have lasted a few hours in which most spectroscopic scans were good, and in which identical conditions hours or days apart led to nearly indistinguishable data sets. More typical is the condition in which the arc drifts from a stable condition into one which has some wobble associated with it and later is stable again. If the arc is in this mode, the column is scanned back and forth continuously, and all other arc data is taken for each scan in the time interval of one scan

(1.5 sec.). Then the data to be analyzed is taken from the middle of the interval during which the arc has remained stable for a few minutes. In comparing raw data taken in this mode of operation, good repeatability is also found.

In contrast to the above difficulties, it is easy to monitor and achieve air purity in the test section, and when properly blanketed with argon, the electrodes have excellent protection. Besides the side-on optical projection of the test section, it is also possible to observe the arc axially through the hollow anode. In addition the breather ports used in the control of the argon-air interface allow a side-on projection of the light near the cathode and anode. In setting up the flow conditions, these auxiliary projections are quite valuable gross monitors of the location of the air and argon, due to different colors of emission from the two gases, and different column diameters, and also indicate the location of any instabilities. Independent control of the flows into the anode and cathode region and into the test section then allow one to approach a good working condition. The final check on purity is done by monitoring the strong argon, oxygen, nitrogen, and tungsten lines spectroscopically. No tungsten or copper lines have been found in the air arcs when operating normally. An additional coarse check is available, since if a tiny water leak develops, a green deposit is found on the plates, and the data becomes suspect. Also, the arc turns red if enough water vapor is present during arc operation.

To check against the possibility of the gas flow affecting the data, the air flows are changed a factor of two or more, above and below normal operating flows. The minimum air flow condition in this test is nearly the condition in which the strongest argon line just begins to increase dramatically in intensity. All the electrical and optical data appear to be little affected by such tests. To test whether the minimum air flow (to achieve purity) is already excessive, the following test was made (Ref. 13). A pure nitrogen arc was established with no flow injection, and only nitrogen (no argon) in the pressure vessel. Optical and electrical data of the nitrogen arc were then monitored as additional nitrogen was fed into the test section at a rate equivalent to the air flow in a typical air arc experiment. Again the changes in the raw data were minor.

A good indicator of the lack of axial non-uniformities in the test section is the linear change in the voltage of the cascade plates as a function of the axial position of the plate. This information is taken frequently, for it also serves as a monitor of the condition of the test channel. Where the gas changes from air to air-argon or pure argon, the gradient in the column voltage also changes.

It has been possible to monitor the stability and symmetry of the arc column by means of the main optical system including the spectrometer. Since the image of the arc at the spectrometer entrance slit is typically 5-10 mm wide, whereas the entrance slit is 30 microns, the excellent spatial resolution and the fast response of the phototube circuit allow the detection of any slow or fast instabilities. In addition the voltage difference between two plates in the test section, and the arc current are monitored by a fast oscilloscope.

The scan of the arc image across the entrance slit takes 1.5 seconds. For a typically good scan, the signal to noise ratio on the chart recorder approaches 50, and the lateral intensity profile is symmetric when folded about

its center, to a degree hidden only by the small noise level on the main signal. If a slight physical wobble of the arc, visible to the eye, is present, then the lateral intensity profile has an apparent higher frequency profile imposed upon the main profile, with an amplitude typically 1/4 to 1/2 of the main profile, and this scan is not used in analysis.

In the work so far, the anticipated possible spectroscopic problems have not proven difficult. Air purity has been easy to achieve, without flow effects, and several strong oxygen and nitrogen lines have been usable in the deduction of temperature profiles which agree well (within 2%) which is comforting. The original equipment was used to examine lines in the 400 to 500nm region. These lines were found to broaden too quickly as the pressure was increased. Additional equipment was purchased to examine the lines near 800 to 900nm. Fortunately, again several oxygen and nitrogen lines were found to be usable to pressures beyond 30 atm. The temperature profiles from the higher wavelength lines were checked against the temperature profiles from the lower wavelength lines, at low pressures. Most of the final data were gathered using the oxygen 844.6nm line, which is a very strong emitter in a region of the spectrum containing no adjacent lines. Even at 30 atm. the "wing" correction for this line is negligible when the spectrometer is set to detect all wavelengths emitted by the line. The checks on the raw data for determining the degree of optical opacity, as described by Griem (Ref. 11) show that this line is still optically thin at 30 atm.

EXPERIMENTAL RESULTS

As discussed in the two preceeding sections the apparatus was constructed and operated so that a steady, cylindrically symmetric, pure air arc column, without axial non-uniformities, could be studied in accordance with the Theory section. Data was taken at 1 atm. for comparison with the results of other laboratories. Then original data was obtained at 6 atm. and 30 atm.

ARC CHARACTERISTICS

The arc characteristics $E_1(I_1)$ for the measurements analyzed herein are shown in Figure 7. The data at 1 and 6 atm. were taken in a channel of 4mm. diameter, the 30 atm. data with a 3mm. diameter.

TEMPERATURE PROFILES

The absolute line intensity technique (Ref. 11, 13) was used to determine the radial temperature profile. With the set-up shown in Figure 6, the chordal intensity of the plasma radiation over a narrow wavelength band was recorded as a function of the distance of the chord from the arc center. This intensity was calibrated against a standard lamp. For one lateral scan, the spectrometer is set to intercept all the radiation from the 844.6nm Oxygen I line plus the continuum radiation at the same wavelength. For the following scan, the continuum radiation at 847nm is measured. Examples of these two scans are given in Figure 8 for the scan at 30 atm., 10.18 amp. Note that the peak continuum intensity (through the arc center) is about 5% that of the peak line intensity, a typical number. On the left is an attempt to get better wing information by changing the recorder gain. Other scans used for careful symmetry checks do not contain this feature.

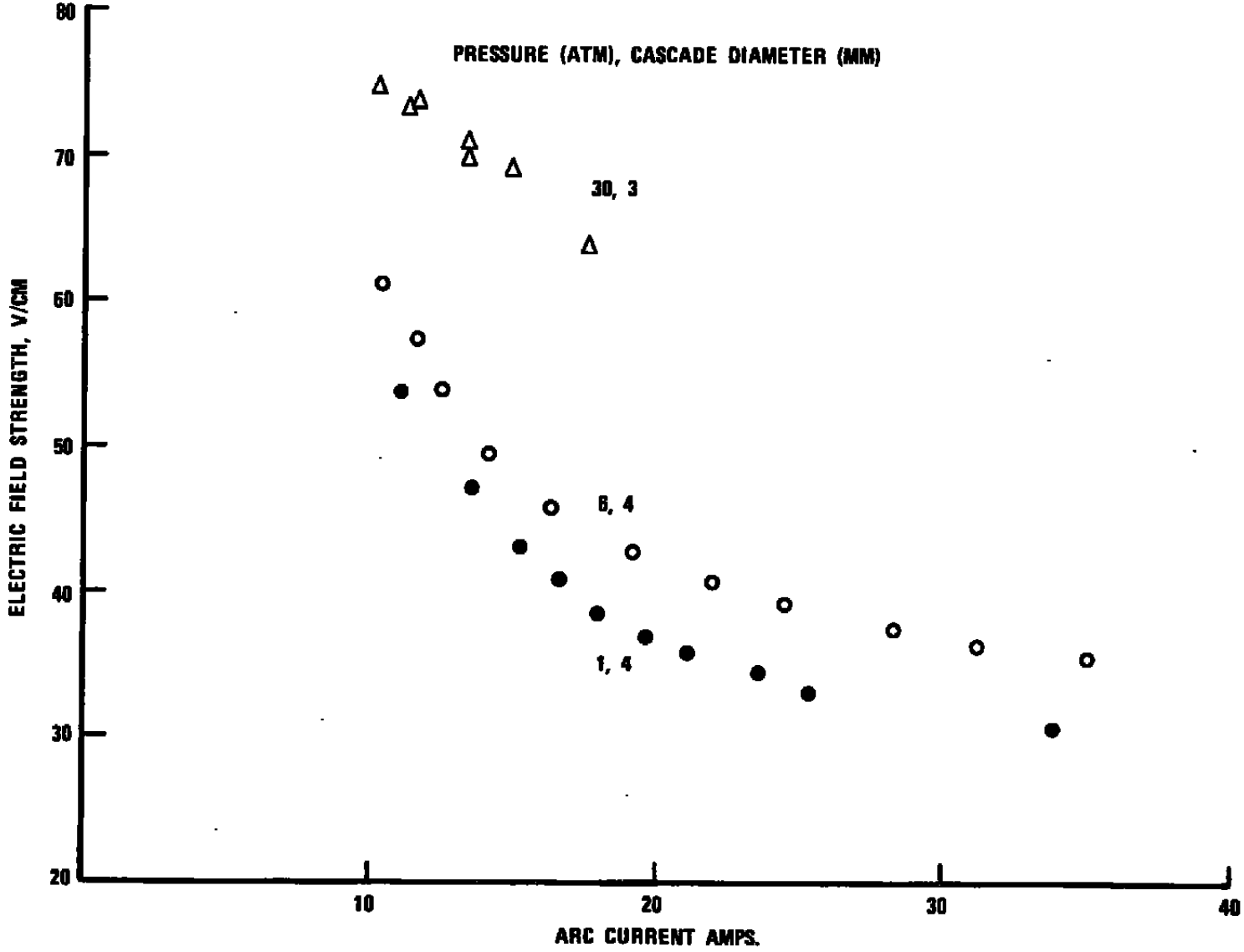

Figure 7. Arc Characteristics E(I,P) for Air

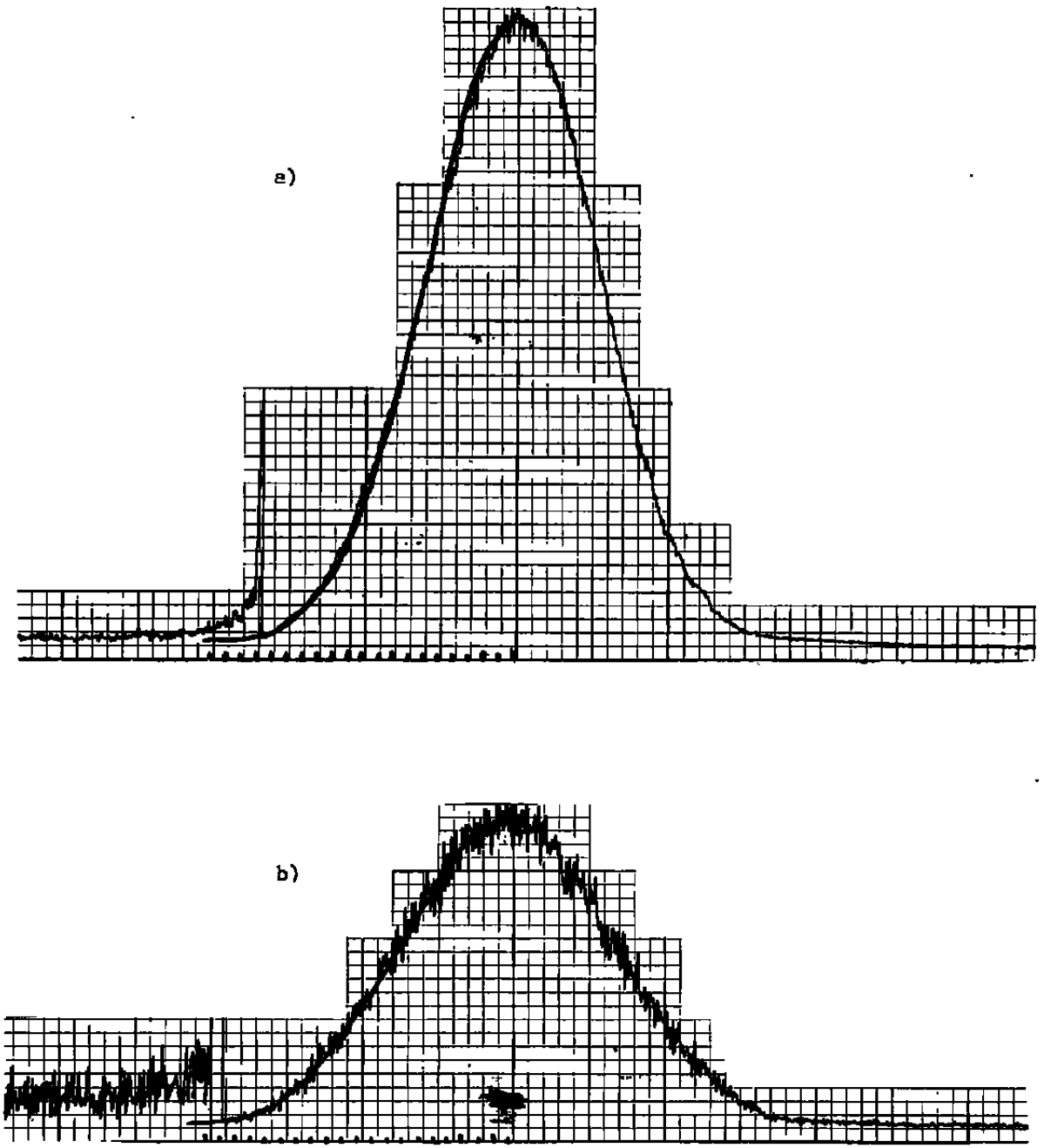

Figure 8. Lateral Intensity Profiles: a) $I_\ell(y) + I_c(y)$ at 844.6 nm; b) $I_c(y)$ at 847 nm. $\Delta\lambda^{\frac{1}{2}}$ = 1.34 nm, relative vertical scale a/b = 10/1, p = 30 atm., I = 10.2 amp., run 274.

The two scans are divided into 40 zones (chordal positions in the arc) and after applying the calibration factos to arrive at absolute intensities, the lower scan is subtracted from the upper. The result is the absolute intensity of the OI 844.6nm line as viewed along chords at different positions. This information is given to the computer to perform an Abel integral inversion (Ref. 11) and arrive at the line emission coefficient $\epsilon_\ell(r)$, radiated power per unit volume at the radius, r.

The Abel inversion program had been developed by Thompson (Ref. 15) who then applied it to the air arc research project. The thompson program has several optional features, including capabilities with semi-optically-thin-arcs.

Within the program, the calculated $\epsilon_\ell(r)$ are then used to calculate T(r) as in Ref. 11. The composition data was taken from Predvoditelev (Ref. 16), the partition function and the lowering of the ionization potential from Drawin (Ref. 17), and the atomic line data from the National Bureau of Standards (Ref. 18). The theoretical values of $\epsilon_\ell(T)$ for the OI 844.6nm line are shown in Figure 9. The temperature profiles so determined from the absolute lateral intensity profiles using the 844.6nm OI line are plotted in Figures 10, 11 for the 180 series, 1 atm. arcs; in Figures 12, 13 for the 210 series, 6 atm. arcs; and in Figure 14 for four of the 270 series, 30 atm. arcs. The general pattern is that as the arc current is increased, the temperature increases at all radii, more so near the arc center. The fact that the gradient is not always zero near the arc center is a common peculiarity of Abel inversion programs. The wiggles near the arc edge are partly due to the Abel program, partly due to reading errors or scattered light in the small-signal wings of the lateral intensity profiles. (See Figure 8). Some comments will be made as to the seriousness of the anomalies in the error analysis section.

ELECTRICAL CONDUTIVITY

The temperature profile $T_i(r)$, current I_i, and field strength E_i were measured for N arcs of different currents (i.e., temperatures). A trial function $\sigma(T)$ was initially assumed. This function was converted to $\sigma_i(r)$, the electrical conductivity as a function of radius for the ith arc, using the measured temperature profile $T_i(r)$ for that arc. Since

$$\frac{I}{\pi E} = 2 \int_0^R \sigma(r) r \, dr \tag{2}$$

A comparison function CF can be defined by

$$CF = \sum_{i=1}^{N} \left(\frac{I_i}{\pi E_i} - 2 \int_0^R \sigma_i(r) r \, dr \right)^2 \tag{3}$$

A computer program, ELCON, has been written which continues to modify $\sigma(T)$ until the minimum value of CF is found. As Devoto (Ref. 10) points out, the criteria for best fit has not been established rigorously. Here an additional cirtical evaluation is applied to CF_{min} by examining the quantity

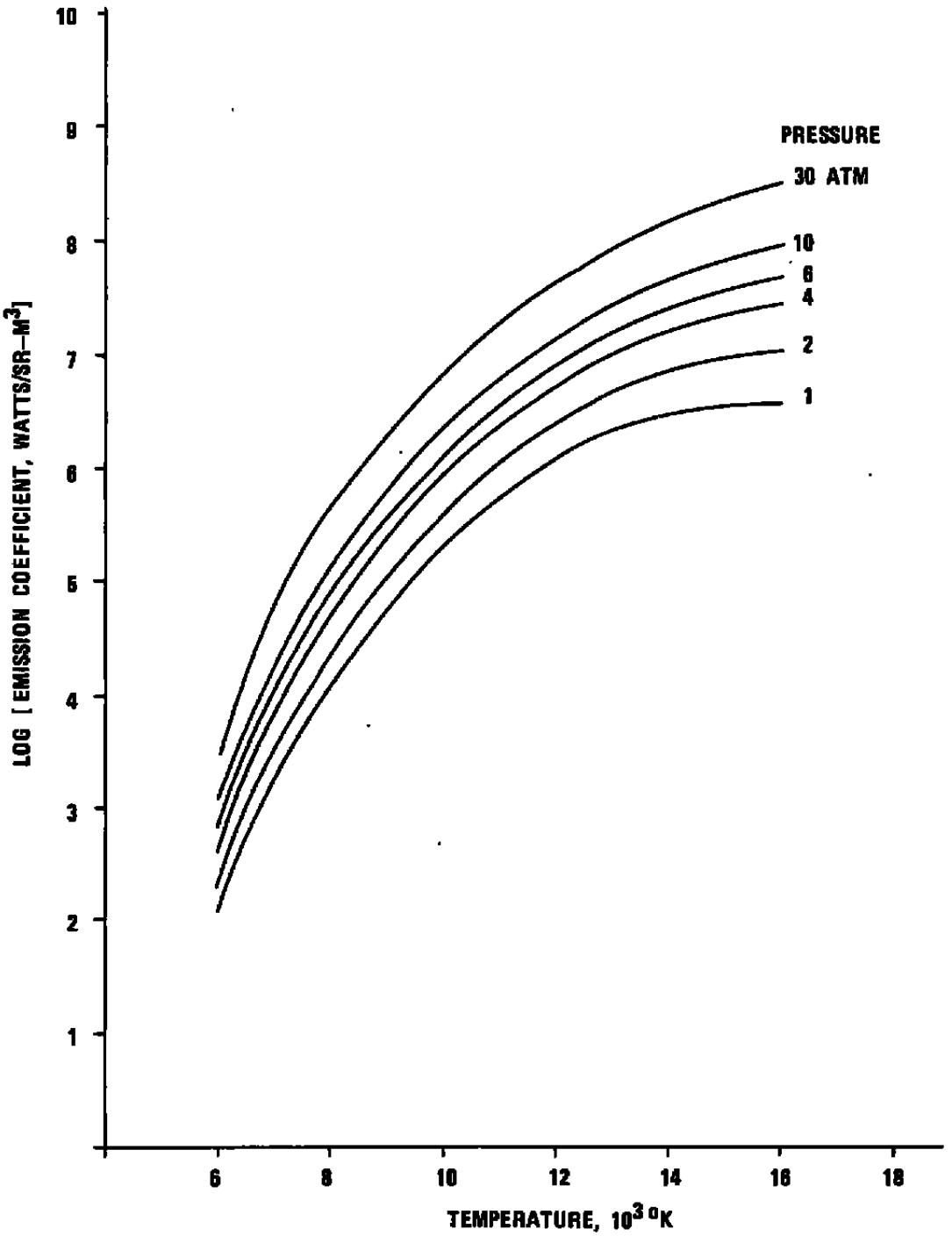

Figure 9. Emission Coefficient of the 844.6 nm Oxygen I Line in Air Plasma.

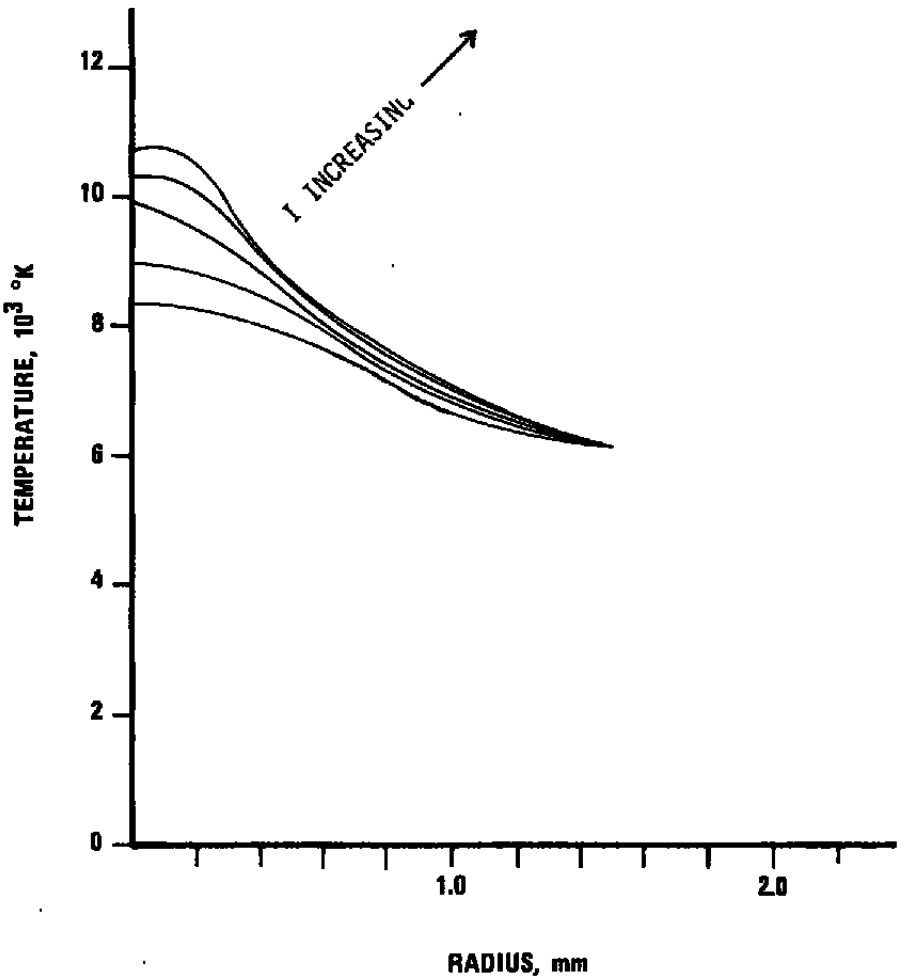

Figure 10. Temperature Profiles in Air Arc at 1 ATM. currents of 11.1, 13.6, 15.2, 16.5, and 18.0 amp., channel wall at 2.0 mm.

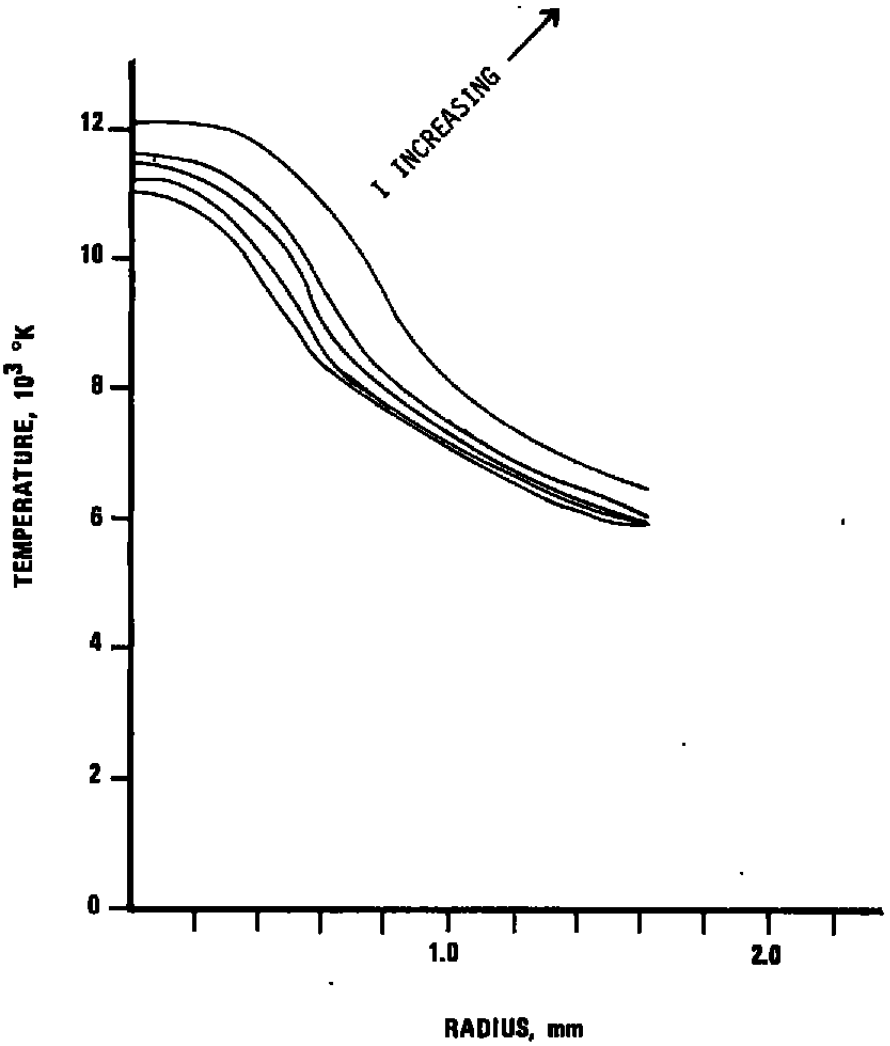

Figure 11. Temperature Profiles in Air Arc at 1 ATM. currents of 19.5, 21.0, 23.5, 25.3, 33.9 amp., channel wall at 2.0 mm.

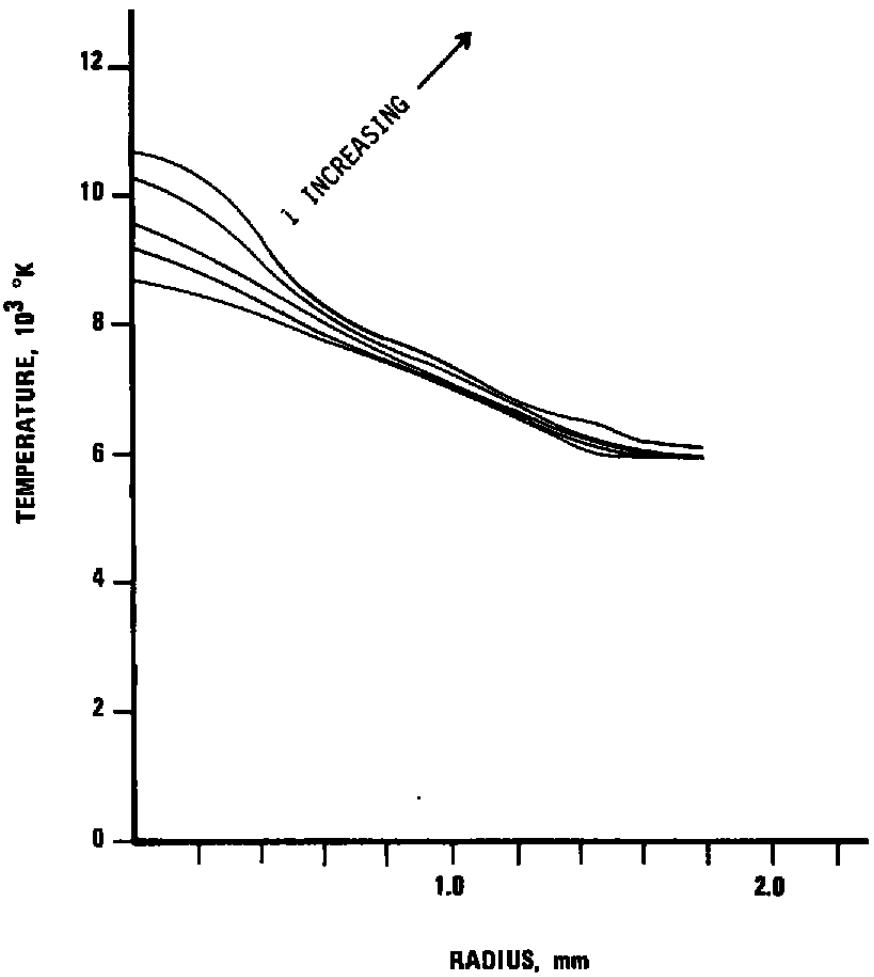

Figure 12. Temperature Profiles in Air Arc at 6 ATM. currents of 10.5, 11.6, 12.6, 14.3, 16.3 amp., channel wall at 2.0 mm.

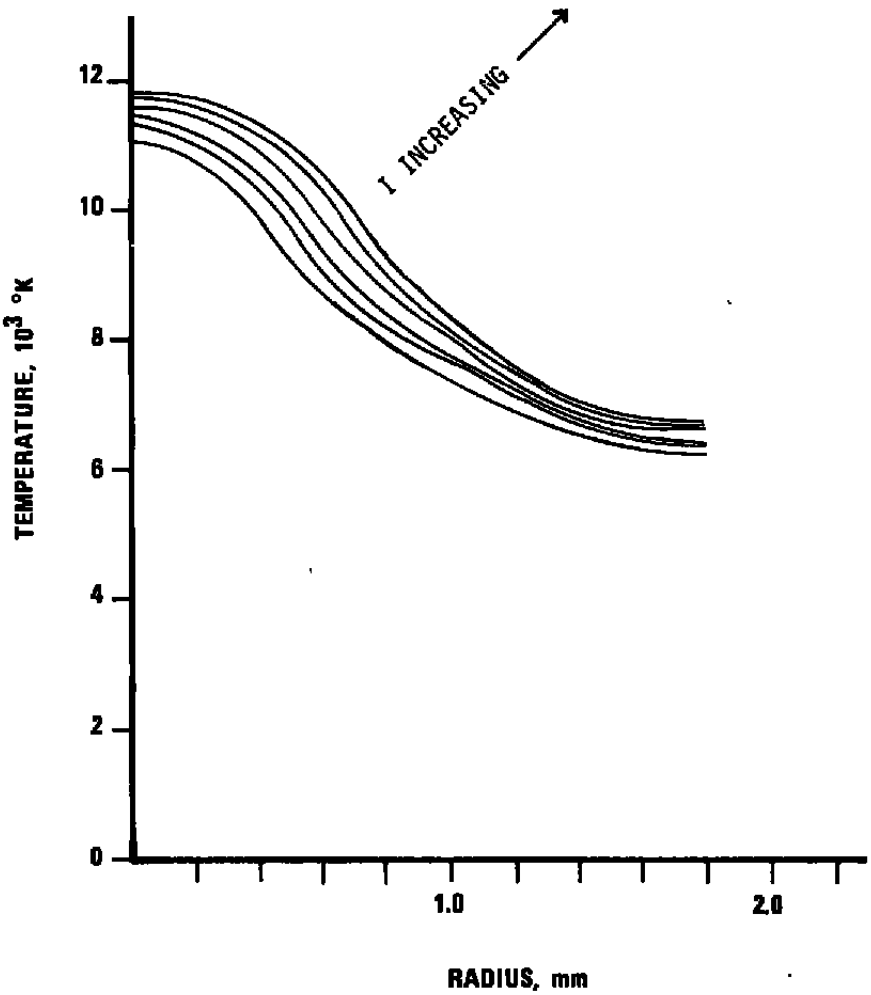

Figure 13. Temperature Profiles in Air Arc at 6 ATM, currents of 19.1, 21.9, 24.4, 28.2, 32.1, 35 amps., channel wall at 2.0 mm.

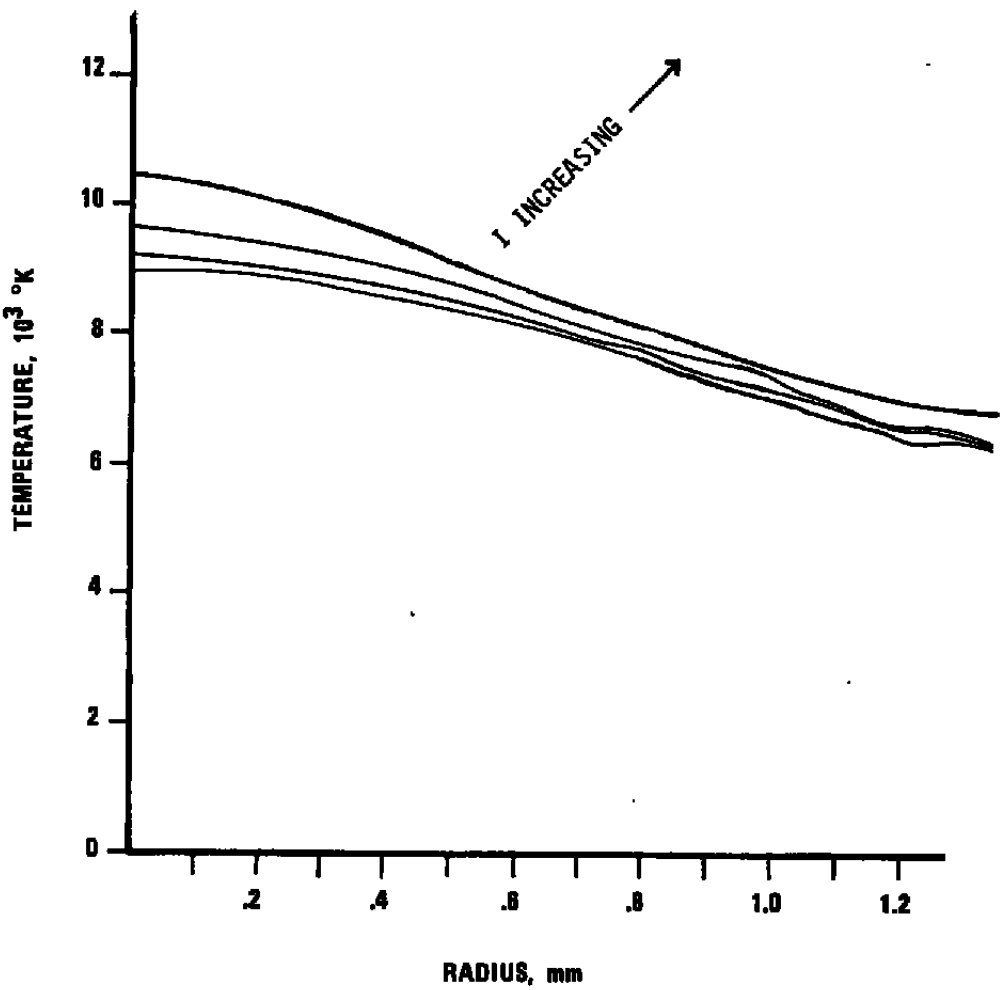

Figure 14. Temperature Profiles in Air Arc at 30 ATM. currents of 10.2, 11.2, 13.2, 17.5 amps., channel wall at 1.5 mm.

$$\Delta \equiv \frac{\frac{I_i}{\pi E_i} - 2\int_0^R \sigma_i^*(r)rdr}{\frac{I_i}{\pi E_i}} \times 100\% \qquad (5)$$

for each arc condition, i, where σ* derives from the trial function which minimizes CF. Using eq. (5), the deviation of the predicted values from the experimental values I_i/E_i can be studied over different temperature ranges, since as I increases, T(r) increases at all radii. Such an evaluation is very helpful in judging the suitability of the trial function and in minimizing the computer time.

Trial functions which have been examined include cubic and quartic polynomials and the function

$$\sigma = BT^{-C} \exp(-D/T) \qquad (6)$$

as suggested by Devoto (Ref. 10) . The work using eq. (6) is presented in this report.

The results of the analysis for the "best fit" of the electrical conductivity are presented in Tables 2,3, and 4. A table is presented for each set of data at pressures of 1, 6, and 30 atm. The rows represent data for each arc condition. The first column gives the arc current, I. Thereafter, successive columns give the axis temperature, T_A; the integral cut-off temperature, T_L; the integral $2\int_0^R \sigma rdr$; the experimental values of $I/\pi E$; and the calculations given in eq. 5. Also tabulated are the coefficients B, C, D for the trial function, and σ(T) using these coefficients. The range of temperature for σ is limited to a range over which significant data is available.

The σ(T) from those tables is compared to existing literature in Figures 15-17. The first is a comparison of theoretical and experimental data at 1 atm. In Figure 16, σ(T) at 6 atm. is compared to theoretical data at 6 and 10 atm. In Figure 17, σ(T) at 30 atm. is compared to theory at 30 and 100 atm.

RADIATION SOURCE STRENGTH

The radiation measurements done so far are incomplete in three ways. First, the wavelength has been limited by the cut-offs of the fused silica windows. Therefore the reported total intensities do not include the expected ultraviolet component. (Ref. 1, 4, 7) Secondly, there is an uncalibrated absorption in the gas between the arc and the outer vessel window. It is known that for the 30 atm. experiments the absorption is 10-20% of the signal at 600-800nm and gets progressively greater as the wavelength decreases. Thirdly, the checks on self-absorption for radiation within the arc have been carried out only at the 844.6nm wavelength used for the temperature determination.

Since the gas absorption would be far less at 1 atm. and the self-absorption is regarded as negligible at 1 atm. (Refs. 1, 4, 7) the analysis was continued, even with incomplete radiation measurements, for heuristic purposes. In what follows, then, Pr (power/length) and u (power/volume) cover the wavelengths passed

TABLE 2

Derivation of the Electrical Conductivity at 1 Atm.

Run Code	Current (Amp.)	T_A (°K)	T_L (°K)	$2\int_0^R \sigma r\, dr$ (calc.)	$I/\pi E$ (exp.)	Δ, Eq. 5 (%)
150	15.1	9,886	6,220	.115	.114	-0.7
151	20.1	11,038	6,484	.168	.176	+4.5
152	23.4	11,903	6,427	.205	.218	+6.2
153	31.0	12,056	6,926	.337	.317	-6.5
154	34.6	12,584	6,974	.355	.363	+2.2
155	40.7	12,970	7,186	.438	.442	+8.6
182	11.1	8,295	6,080	.102	.066	-56.
180	13.6	8,908	6,232	.088	.092	+4.4
181	15.2	9,993	6,099	.108	.118	+3.5
183	16.5	10,320	6,244	.118	.128	+7.3
184	18.0	10,662	6,216	.128	.148	+1.3
185	19.5	11,009	6,002	.157	.166	+5.0
186	21.0	11,185	6,128	.177	.177	-0.5
187	23.5	11,525	6,002	.203	.218	+6.9
188	25.3	11,610	6,050	.238	.241	+1.3
189	33.9	12,186	6,675	.371	.351	-5.5

$$\sigma = B\, T^{-C} \exp(-D/T)$$

B = 1.01035 E+12
C = 1.96022 E+00
D = 6.31783 E+04

T (°K)	σ (Mho/cm)
6,500	2.04
7,000	3.53
7,500	5.63
8,000	8.39
8,500	11.9
9,000	16.0
9,500	20.8
10,000	26.3
10,500	32.3
11,000	38.7
11,500	45.5

TABLE 3

Derivation of the Electrical Conductivity at 6 Atm.

Run Code	Current (Amp.)	T_A (°K)	T_L (°K)	$2\int_0^R \sigma r\, dr$ (calc.)	$I/\pi E$ (exp.)	Δ, Eq. 5 (%)
210	10.5	8,646	6,015	.050	.055	+8.0
211	11.6	9,038	6,017	.058	.064	+9.9
212	12.6	9,534	6,023	.069	.074	+7.0
213	14.4	10,258	6,069	.089	.092	+3.0
214	16.3	10,734	6,045	.114	.113	-1.0
215	19.1	11,076	6,152	.146	.141	-3.1
216	21.9	11,346	6,235	.181	.170	-6.8
217	24.4	11,451	6,329	.186	.196	+5.2
218	28.2	11,516	6,491	.231	.239	+3.1
219	32.0	11,613	6,338	.287	.278	-3.0
221	35.1	11,709	6,501	.310	.311	+0.5

$$\sigma = B\, T^{-C} \exp(-D/T)$$

B = 9.6182495 E+11
C = 1.8367218 E+00
D = 7.5527820 E+04

T (°K)	σ (Mho/cm)
6,500	.858
7,000	1.72
7,500	3.11
8,000	5.18
8,500	8.07
9,000	11.9
9,500	16.8
10,000	22.7
10,500	29.7

TABLE 4

Derivation of the Electrical Conductivity at 30 Atm.

Run Code	Current (Amp.)	T_A (°K)	T_L (°K)	$2\int_0^R \sigma r\, dr$ (calc.)	$I/\pi E$ (exp.)	Δ, Eq. 5 (%)
274	10.2	8,972	6,391	.043	.044	+0.6
275	11.3	9,130	6,302	.048	.049	+3.6
270	11.7	9,327	6,220	.050	.051	+0.9
271	13.1	9,587	6,705	.061	.059	-3.4
276	13.3	9,616	6,314	.059	.061	+3.0
272	14.8	9,857	6,784	.073	.069	-6.4
273	17.6	10,474	7,044	.085	.088	+3.0

$$\sigma = B\, T^{-C} \exp(-D/T)$$

B = 2.29315 E+12
C = 1.82923 E+00
D = 8.62743 E+04

T (°K)	σ (Mho/cm)
6,500	.418
7,000	.942
7,500	1.89
8,000	3.45
8,500	5.82
9,000	9.21
9,500	13.8
10,000	19.8

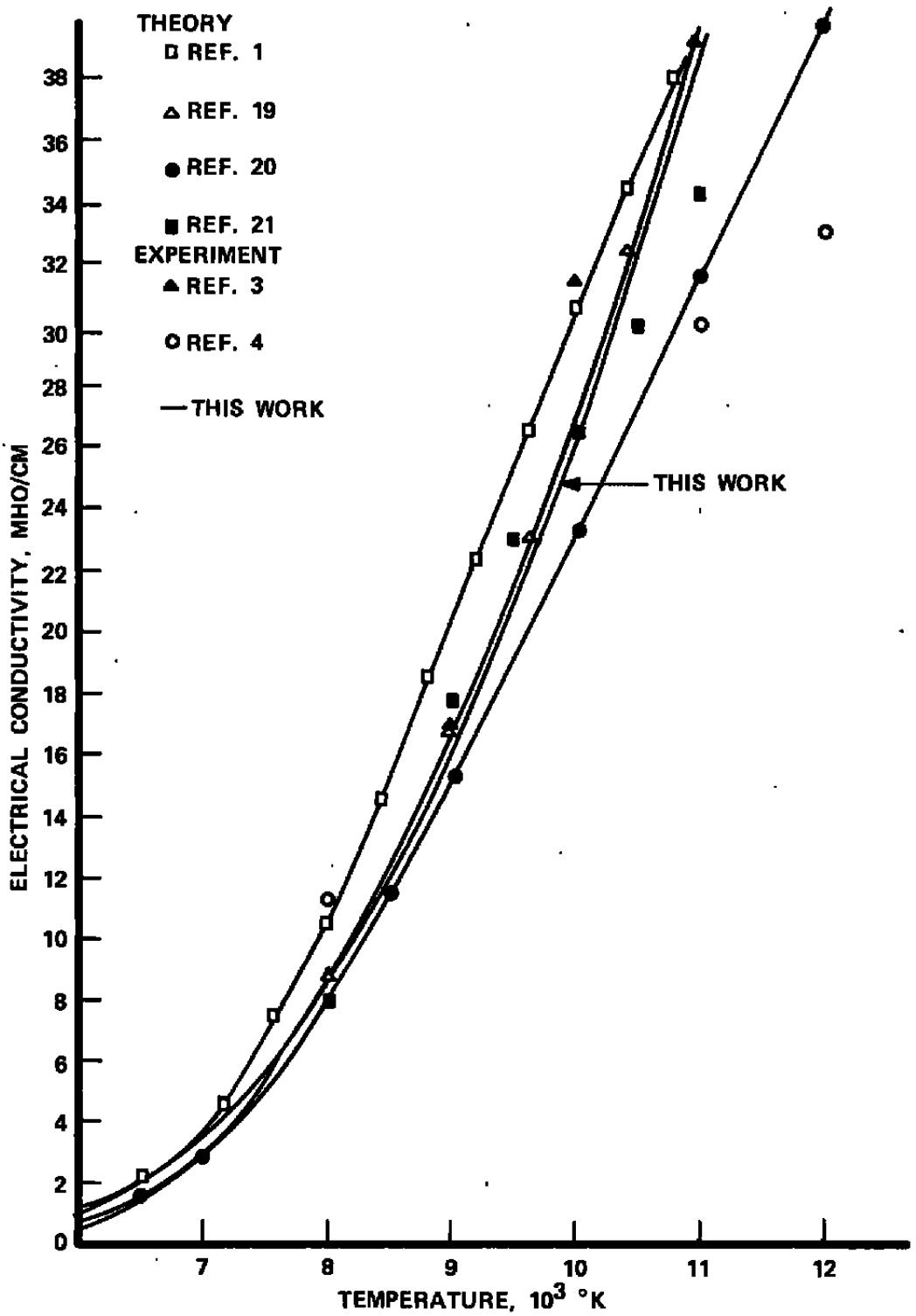

Figure 15. Electrical Conductivity of Air Plasma at 1 Atm.

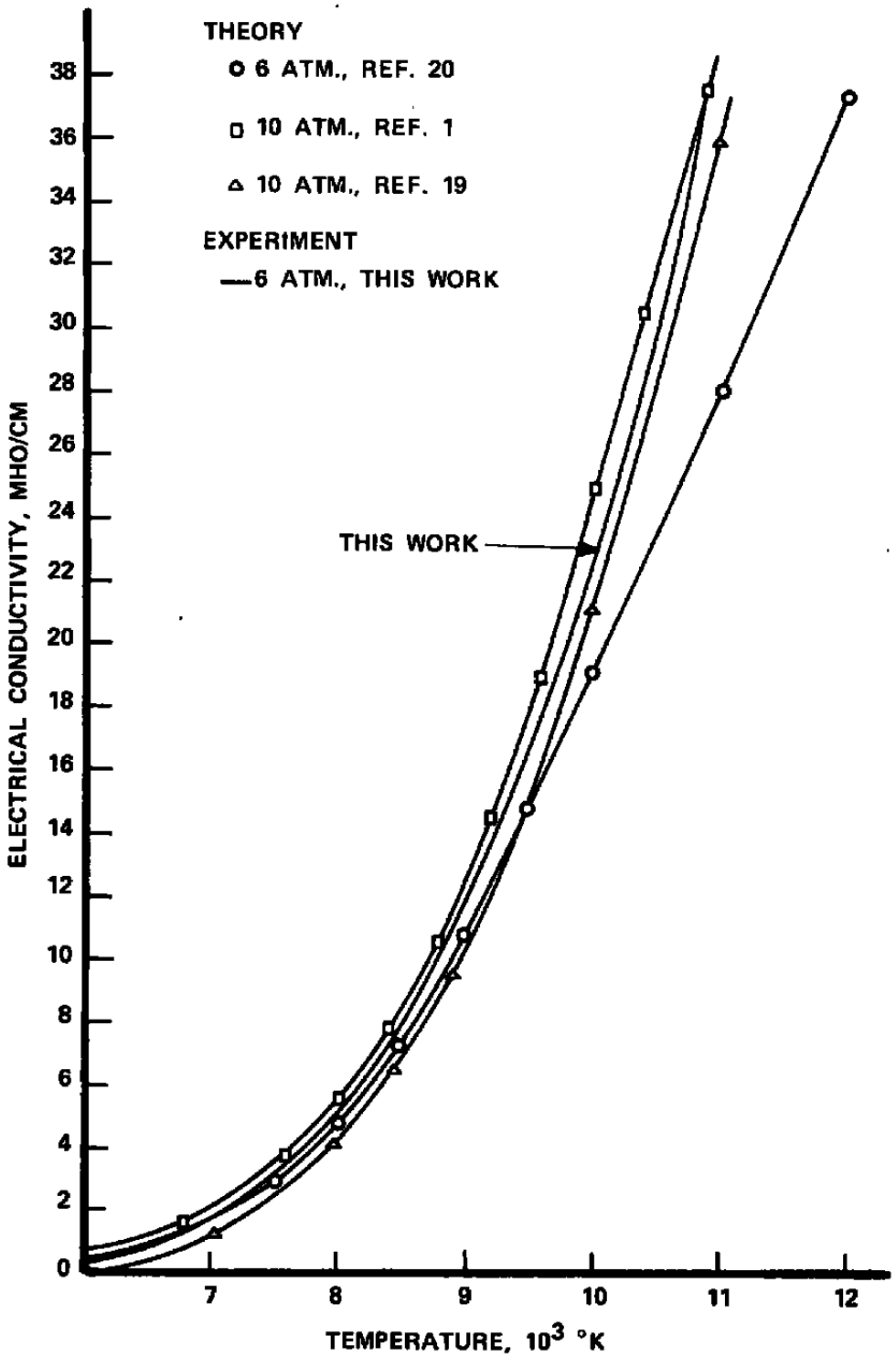

Figure 16. Electrical Conductivity of Air Plasma at 6 Atm.

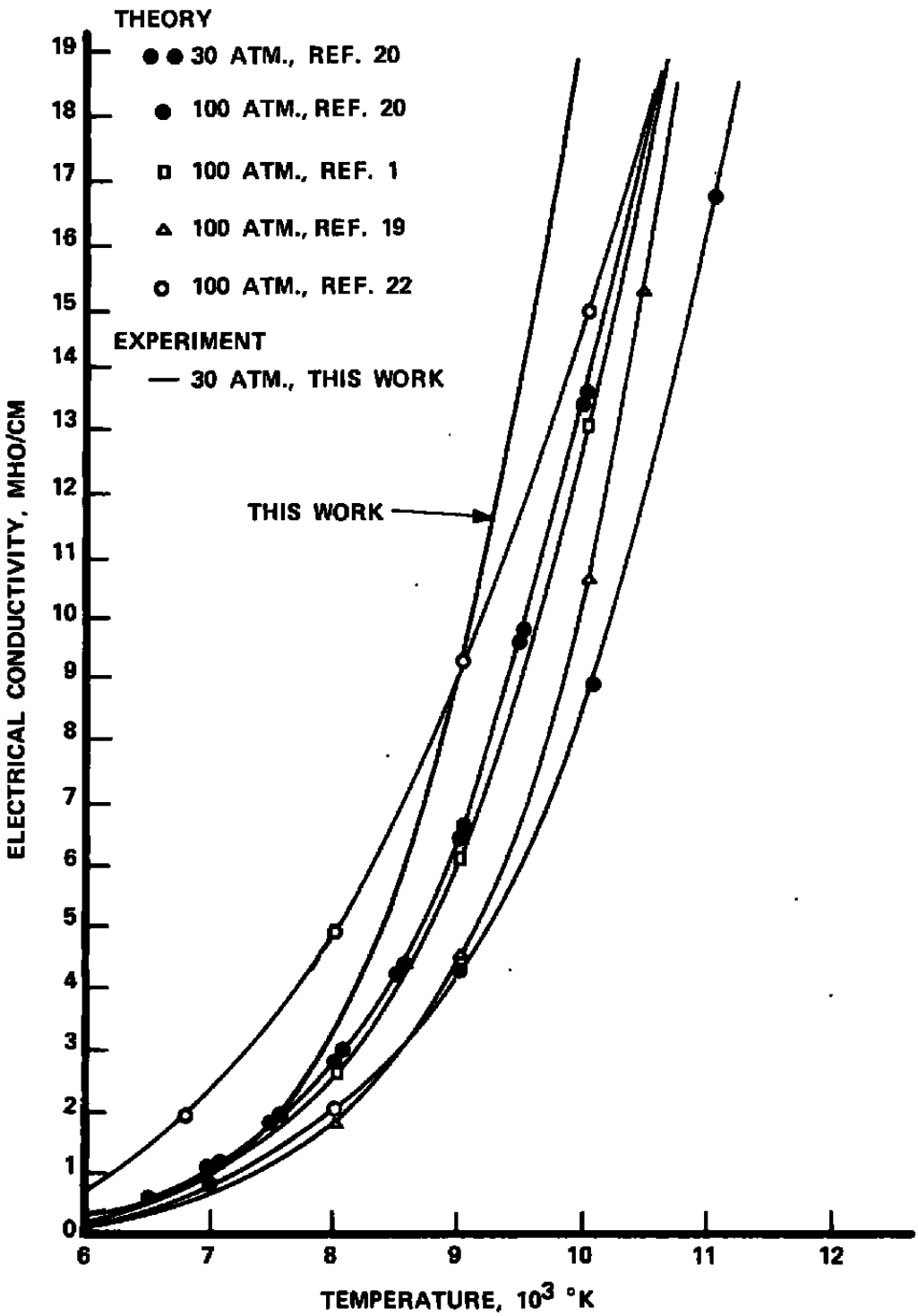

Figure 17. Electrical Conductivity of Air Plasma at 30 Atm.

by fused silica windows, and self-absorption and gas absorption are ignored. If self-absorption is important, Pr still retains physical significance as the radiation escaping from the arc, but the deduction of u would be in error.

For an optically thin arc, the technique for deducing u(T) in eq. (3) is the same as that described above for deducing $\sigma(T)$ in eq. (2). The total radiant energy P_r was measured by observing a known "slice" of the arc with a calibrated thermopile. If a thermopile with a rectangular receiving area views an arc column through a rectangular slit, it can be shown that

$$P_r = \frac{4\pi\ X_S\ X_A}{AS\tau}\ P_* \tag{7}$$

where

P_* is the power received by the thermopile

X_S is the distance between the thermopile and the slit

X_A is the distance between the thermopile and the arc center

A is the thermopile receiving area

S is the slit height

τ is the transmission of the vessel and cascade windows

provided that the dimensions of the thermopile, the slit, and the viewed arc column are small compared to X_S.

The measured radiated power per unit length is given in Figure 18 as a function of arc current for a pressure of 30 atm. One data point is also given at 6 atm. and at 1 atm. For comparison, EI/10, one-tenth of the electrical power input per unit length is also plotted. It is seen that the measured radiated power is only a few per cent of the electrical input power.

The radiation source strength for an optically thin arc is related to P_r (power/unit length) by

$$P_r = 2\pi \int_0^R ur\ dr. \tag{3}$$

Using the experimentally measured temperature profile $T_i(r)$, a trial function, u(T), was converted to $u_i(r)$ and the integral evaluated. In a series of arcs with different currents, using $T_i(r)$, P_{ri} for each arc, the comparison function

$$CF_{rad} = \sum_{i=1}^{N} \left(\frac{P_{ri}}{\pi} - 2 \int_0^R ur\ dr \right)^2 \tag{8}$$

was minimized by a computer code.

Additional criticism was applied to the minimum CF_{rad} by evaluating the deviation

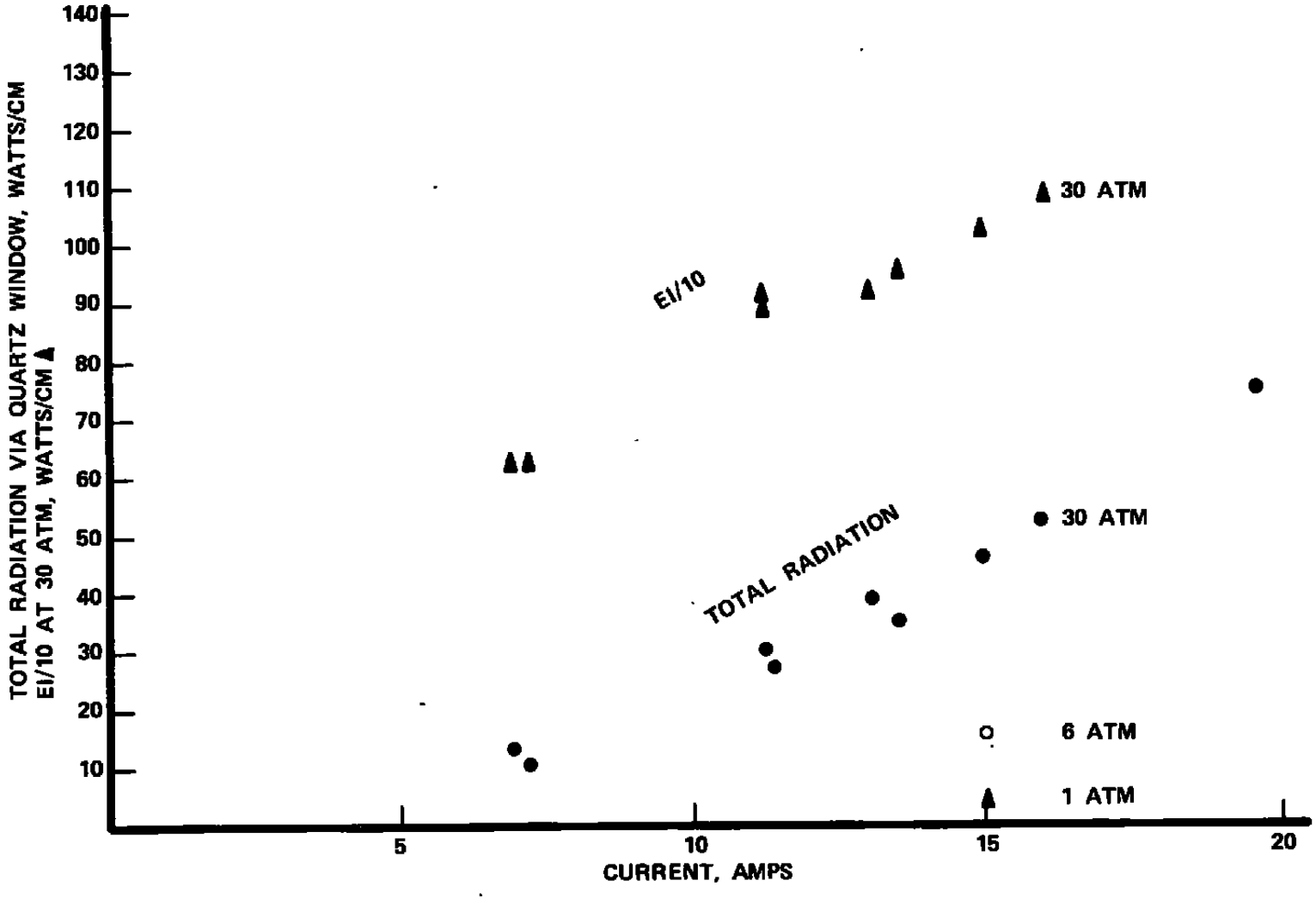

Figure 18. Radiation of Air Arc vs. Current and Pressure.
(30 atm. data are lower limits, see text)

$$\Delta_{rad} \equiv \frac{\frac{P_{ri}}{\pi} - 2\int_0^R ur\,dr}{\frac{P_{ri}}{\pi}} \times 100\% \tag{9}$$

between the predicted values and the experimental values, P_{ri}. A trial function of the form

$$u(T) = BT^{-C} \exp(-D/T) \tag{10}$$

was found to be suitable.

The results for a pressure of 30 atm. appear in Table 5 and Figure 19. In Table 5, the successive columns are: arc current, I; axis temperature, T_A; the integral cut-off temperature, T_L; $2\int_0^R urdr$; P_{ri}/π; and Δ_{rad} (from eq. 9). Also tabulated are the "best fit" values for B, C, D in the trial function above, and u(T) based on those coefficients. The u(T) function is plotted in Figure 19 over the range where significant data is on hand. The value of u(9,000) at 30 atm. is about 38 times greater than measured by Schreiber (Ref. 4) at 1 atm.

THERMAL CONDUCTIVITY

Eq. (1) is used to evaluate the thermal conductivity, k. The functions $\sigma(T)$ and u(T) are determined as in the two preceeding sub-sections. For a given arc (i), the temperature profile $T_i(r)$ is used to express $\sigma_i(r)$ and $u_i(r)$. Thereafter, eq. (1) may be integrated directly to get

$$-\left(\frac{dT}{dr}\right)_i k = \frac{\int_0^R \left[E_i^2\,\sigma_i(r) - u_i(r)\right] rdr}{r} \tag{11}$$

The r.h.s. is evaluated by computer. The gradient $\left(\frac{dT}{dr}\right)_i$ of the temperature profile has so far been determined by hand by plotting $T_i(r)$ on large graph paper.

As noted at the start of the preceeding section, u may be in error due to the omission of the ultraviolet component and the neglect of self-absorption gas absorption. Nevertheless, the analysis is continued for heuristic purposes.

For the analysis of the 30 atm. data, $\sigma(T)$ and u(T) were taken from Tables 4 and 5 respectively. Note that at any radius, u is a few percent of σE^2. For the analysis of the 1 atm. data, $\sigma(T)$ was taken from Table 2, but u(T) had not been determined. The data on P_r in Figure 18 suggests that u(T, 1 atm.) ≈ (.091)u(T, 30 atm.). Thus in comparison to σE^2, omission of u(r) in eq. (11) would cause about a 1% error in the calculation of k(T) at 1 atm. However in the results presented here u(T, 1 atm.) was taken equal to .091 u(T, 30 atm.) as a better approximation. The data on P_r in Figure 18 suggests that u(T, 6 atm.) ≈ .33 u(T, 30 atm.) and this value was used in eq. (11) for the calculation of k at 6 atm.

TABLE 5

Derivation of the Radiation Source Strength at 30 Atm*

Run Code	Current (Amp.)	T_A (°K)	T_L (°K)	$2\int_0^R \sigma r\, dr$ (calc.)	P_r^*/π (exp.)	Δ, Eq. 9 (%)
274	10.2	8,972	6,391	8.1	7.4	-9.1
275	11.3	9,130	6,302	9.2	9.0	-2.6
270	11.7	9,327	6,220	9.8	9.5	-2.9
271	13.1	9,587	6,705	12.4	11.8	-4.3
276	13.3	9,616	6,314	12.0	12.2	+1.8
272	14.8	9,857	6,784	15.4	14.8	-3.8
273	17.6	10,474	7,044	18.8	20.1	+6.0

$$U^* = B\, T^{-C} \exp(-D/T)$$

B = 1.73939 E+13
C = 1.32689 E+00
D = 9.69331 E+04

T (°K)	U^* (Watts/cm^3)
6,500	48.3
7,000	128.
7,500	295.
8,000	605.
8,500	1140.
9,000	1996.
9,500	3270.
10,000	5085.

*Refers to radiation for which quartz is transparent. U and P_r are used for heuristic purposes only since self-absorption and media absorption have not been treated rigorously.

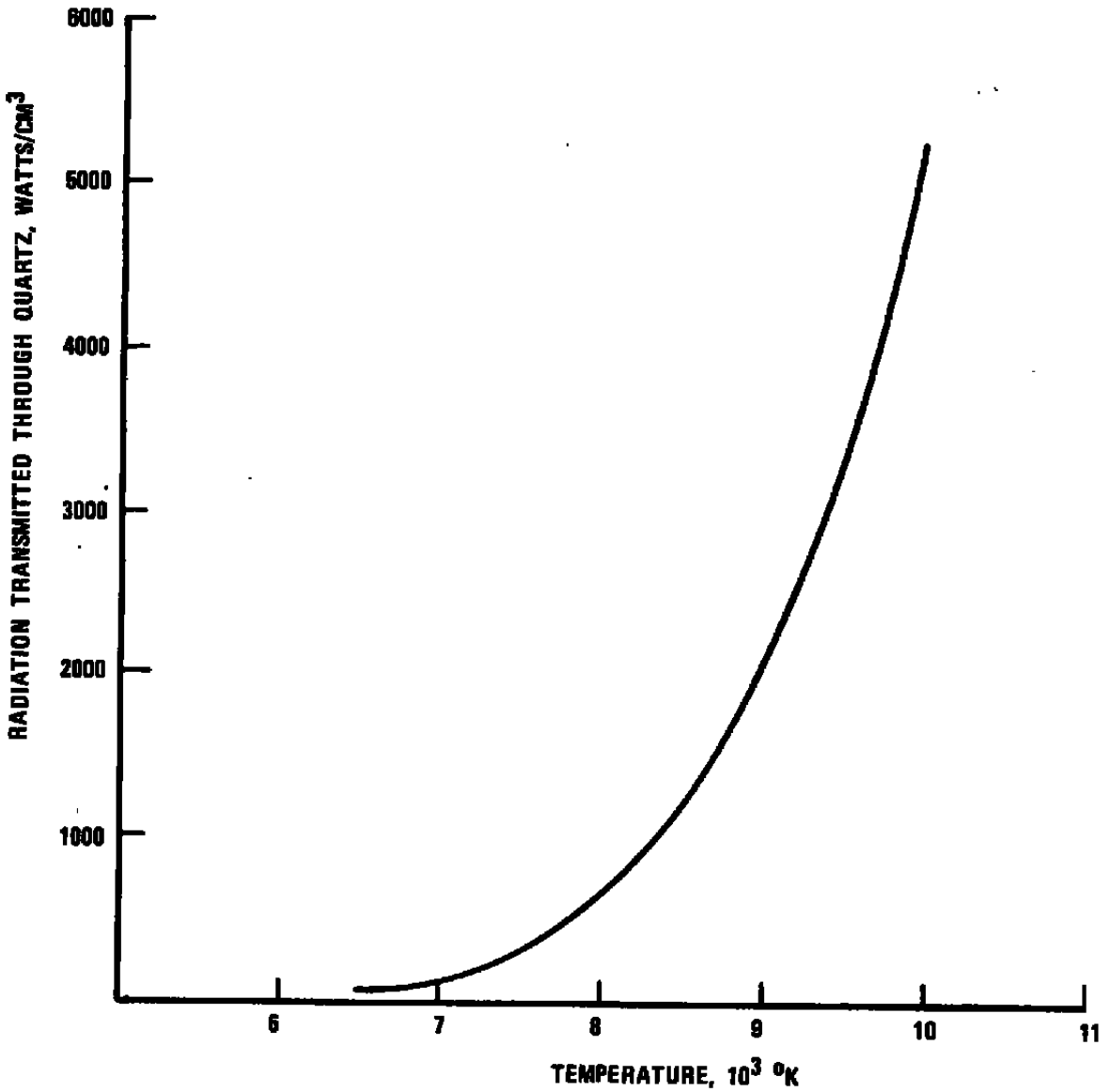

Figure 18. Radiation Source Strength of Air Plasma at 30 ATM. (incomplete data, see p. 30)

The results for the thermal conductivity at 1 and 6 atm. are given in Figure 20 together with recent theoretical calculations (Refs. 1, 19, 20). The experimental data at 1 atm. from Ref. 3 is also plotted. (The earlier theories are compared to that data in Ref. 3). The experimental results at 30 atm. are given in Figure 21 and compared with the theories at higher pressure (Refs. 1, 19, 20).

ERROR ANALYSIS

For the electrical conductivity, the major sources of error lie in the measurement of the electric field strength, the use of the radiation standards, and in the uncertainty of the transition probabilities. (Refs. 7, 14). The latter is 10% for the OI 844.6nm line (Ref. 18). Accounting for the absorption of that line in the gas outside the arc, as measured, would increase the temperatures in Tables 2, 3, 4 by no more than 50°K at 30 atm, far less at 1 and 6 atm. From eq. (4) one can see that $\sigma(T)$ has the best accuracy at temperatures represented by the most arcs, i.e. at the middle temperatures of Figures 15-17. At the lower temperatures the accuracy is poorer because of less data and because the data comes from the edge of the arc. At the highest temperatures, again there is less data, and it is less accurate. As the error analysis is conducted for these experiments, one expects an uncertainty of ±15% for $\sigma(T)$ near the middle temperatures.

The largest uncertainty in the radiation measurements lies in their incompleteness. The ultraviolet component is unknown, and the absorption outside the arc is uncalibrated, except at 844.6nm. Thus Pr in Figure 18 must be taken as a lower limit. In Figure 19, u(T) is similarly to be taken cautiously.

In treating the thermal conductivity, eq. (11) shows that errors in the radiation measurments are less serious for arcs in which u is small compared to σE^2. In either case, a critical factor in evaluating k(T) is the gradient of the temperature profile. The scatter in values from individual arcs is due primarily to inaccuracies in determining the slope. Large errors are possible at the center and at the edge of the arc, and when these approached 100%, the calculations were terminated.

In the integral of eq. (11), as r→R the integral approaches

$$\frac{I_i E_i}{2\pi} - \frac{P_{ri}}{2\pi}.$$

If as in Figure 18, the radiation term is relatively small, and since I_1E_1 has a relatively high accuracy, the k(T) from eq. (11) is better known at larger and larger radii until the inaccuracies of determining dT/dr creep in. Apart from errors due to the measurement of dT/dr, one would expect an uncertainty in k(T) of ± 10% at those temperatures where the scatter is minimum. An overall uncertainty of ± 20% appears to be reasonable for k(T) at the temperatures where the scatter is minimum, but only if u(T) is small.

There is some evidence (Ref. 8) that nitrogen arcs are not in local thermodynamic equilibrium at pressures of 1 atm. and temperatures under 10,000°K. Such problems have not yet been systematically investigated in this program. Temperature profiles measured in the present study, using different atomic transitions, agree well, whereas the non-L.T.E. conclusions (Ref. 8) came from

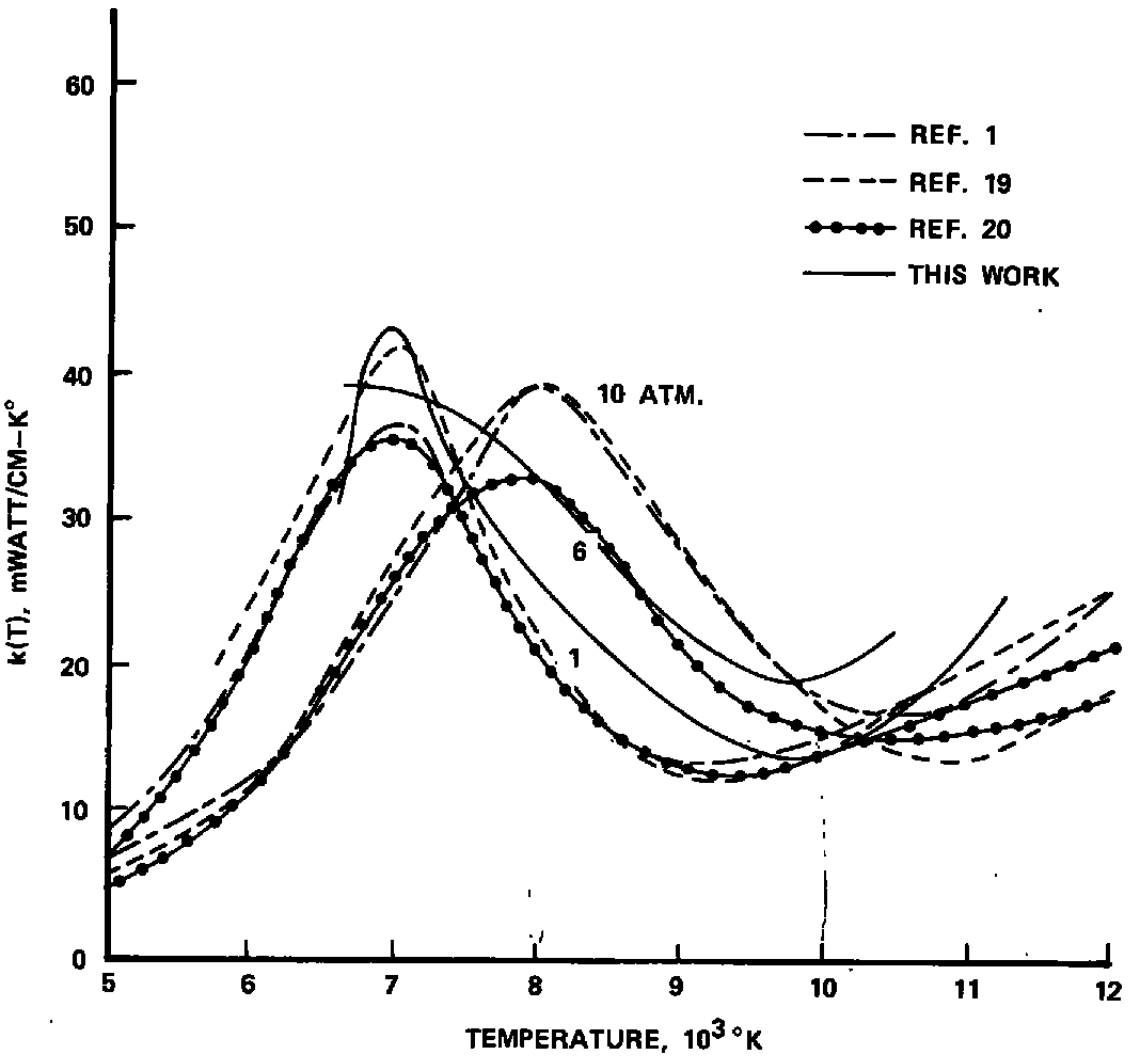

Figure 20. Thermal Conductivity of Air Plasma at 1 Atm. and 6 Atm.

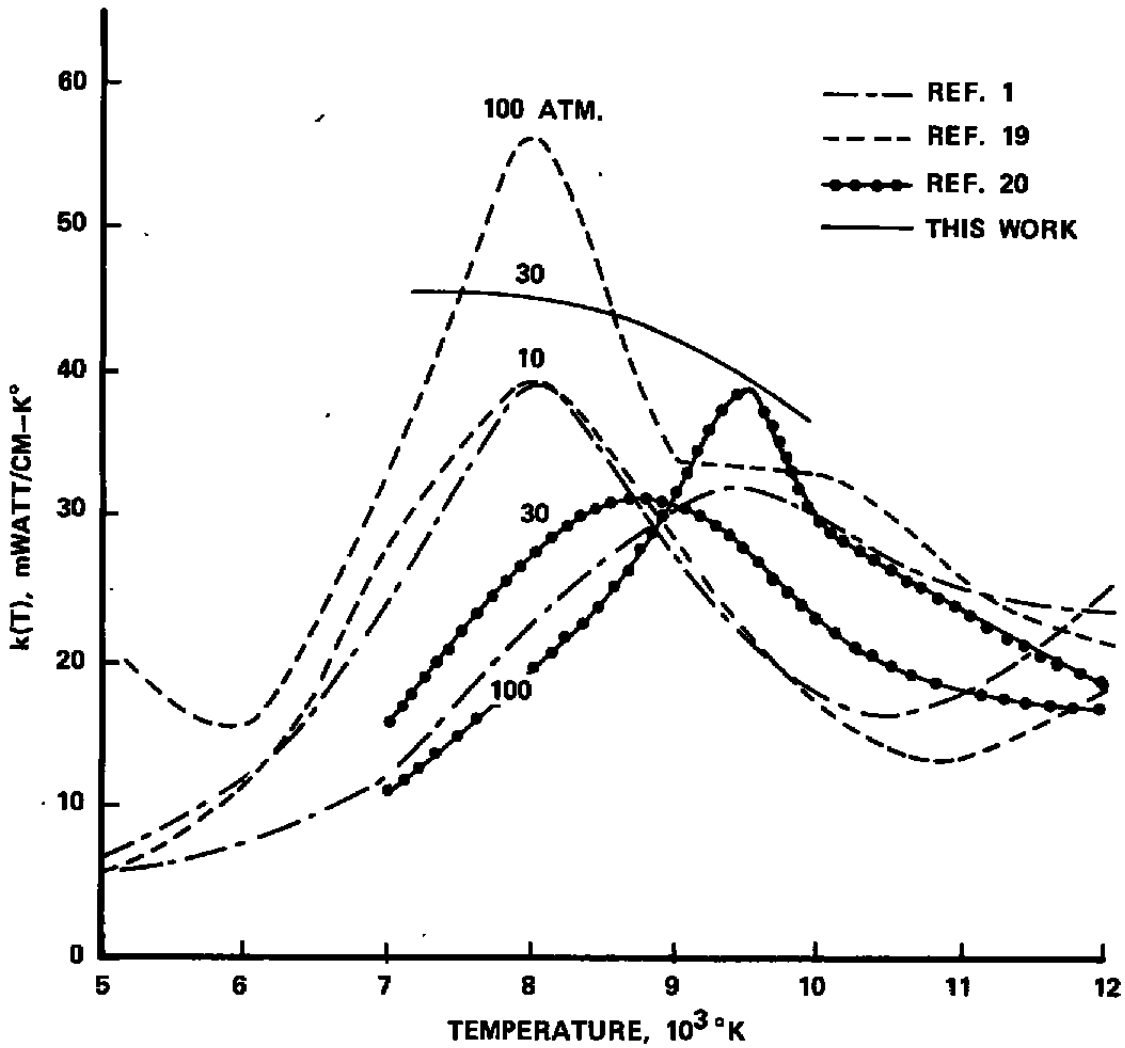

Figure 21. Preliminary Thermal Conductivity of Air at 30 Atm.

comparisons to molecular phenomena. It is generally thought that as current or pressure is increased, L.T.E. occurs more readily, but not at the arc edge.

The results for $\sigma(T)$ and $u(T)$ are rather insensitive to the inaccuracy of the data at the arc edge for two coupled reasons. First, both functions are expected to be rapidly increasing functions of temperature in the range of this study. Secondly, if radiation losses are small, temperature must fall significantly away from the arc center. Thus contributions to the integrals used in this study are rather small near the edge of the column. For the evaluation of $k(T)$, error in the temperature gradient near the edge causes comparable error in $k(T)$. For this reason, $k(T)$ values given in this report do not include data from near the arc edge.

A decision of procedure at the start was to take the raw data straight through all the analyses with as little smoothing of the data as possible. In hindsight, smoothing has a very strong effect on any peak in the thermal conductivity (see Figure 20) due to the presence of the dT/dr factor in eq. (11). Smoothing has a far less effect on the electrical conductivity and the radiation source strength, particularly at temperatures where $\sigma(T)$ and $u(T)$ are presented with greater confidence. An analysis has shown that the large relative errors in the wings of the lateral intensity profiles do not propagate significantly into higher temperature regions of the arc. The best way to reduce the uncertainty in the properties at the extremes of the temperature range now under study is to extend the experiments to higher and lower currents so that the temperatures of interest fall near the middle radii of the arc.

As is evident in Figures 10 to 14, the temperature is unknown near the copper wall because of the low intensity of the OI 844.6nm line. The consequences of such have been examined by analytical extensions of the temperature profiles. The worst case is illustrated in Figure 10. Nearly 44% of the cross-sectional area of the copper channel exists beyond the end of the published profile. However, theory and experiment reveal that $\sigma(T)$ and $u(T)$ fall by a factor ~ 3 for each 1,000°K drop in T. Since T must fall to ~700°K at the wall, the outer region carries little current. It is estimated that inclusion of the outer region in the calculation would change $\sigma(T)$ and $u(T)$ no more than a few percent at the temperature extremes of the data in this report. At the middle temperatures, smaller relative changes would occur.

DISCUSSION AND CONCLUSIONS

The values of the electrical and thermal conductivities at 1 atm. are in excellent agreement with experimental data from other laboratories. The experimental data at 6 and 30 atm. is new. The electrical conductivity compares favorably with theory at 1 and 6 atm., as does the thermal conductivity. At 30 atm. the experimental values of the electrical conductivity at 7,000 to 8,000°K are in agreement with the only theoretical values available (Ref. 20). At 10,000°K, the theoretical data of Ref. 20 are 32% lower. However, the data of Ref. 20 are consistently lower than that of the other theoretical references at 10,000°K, at 1, 6 and 100 atm. by about 25%. The experimental thermal conductivity at 30 atm. is in reasonable agreement with the theory of Sokolova (Ref. 19) but is 50% higher than predicted by Liebermann (Ref. 20) or Nicolet (Ref. 1).

Caution must be used in interpreting the total radiation measurements and in applying them to the deductions of the volume emission coefficients and of the thermal conductivity. So far, no ultraviolet component has been included, and it has been assumed that the arc plasma and surrounding medium are optically thin at all wavelengths. The latter assumption has been verified at 844.6nm for the sake of the temperature profiles and the deduction of the electrical conductivity. However, the surrounding medium at 30 atm. is known to attenuate the radiation significantly at wavelengths below 600nm, but the absolute values of the attenuation have not been calibrated.

The experimental values of the total radiation measurements at 30 atm. may be too low and the thermal conductivity too high due to the incomplete radiation measurements. Because of the resultant uncertainty in the radiation source strength in equation (11), some comments are in order on the good agreement shown by the thermal conductivity to other works, particularly at 1 and 6 atm. (Figures 20 and 21). That the agreement might not be fortuitous can be argued in the following way. First, it is generally expected that the air arc at 1 atm. is optically thin and some work verifies this. (Ref. 3, 4). Secondly, the absorption by the medium outside the arc observed at 30 atm. would be far less at 1 atm. due to the total mass decrease. Thirdly, if $u << \sigma E^2$, then errors in measuring u are not important in deducing the thermal conductivity from equation (11). At 1 atm., the value of u actually used was only 1% of σE^2. At 6 atm., u was about 5% of σE^2.

The arcs studied in this report had center-line temperatures near 11,500°K and below. Some inferences can be drawn for such arcs from Refs. 3, 4, 7 about the third point concerning the relative magnitudes of u and σE^2. Asinovsky (Ref. 3) reports on experiments and calculations done on air arcs of different diameters at 1 atm. which show that radiation is unimportant in equation (1) and (11) for arcs with center-line temperatures below 11,500°K, but is significant for higher temperatures. These conclusions relate to the total spectrum, including any ultraviolet component. Interestingly, his methods rely on measurements of σ, E, and T and do not rely on radiation measurements.

That the value of u(T) used in equation (11) at 1 atm. is not unreasonable can be inferred also from Ref. 4. Schreiber measured the total radiation for $\lambda > 200$nm from an air arc at 1 atm. over the temperature range from $9,000°K < T < 13,000°K$. He also used a non-radiative technique based upon a Hall probe measurement on the arc axis to show that at 12,400°K, the total radiation at all wavelengths was about 2.5 times larger than the radiation for which $\lambda > 200$nm. An interpretation of Schreiber's results suggests the same factor might hold at

the lower temperatures. In the present report the value of u(T) was about 3.5 times the Schreiber measurement for λ > 200nm, and thus u(T) is about 40% greater than the total radiation inferred from Schreiber's work.

Morris (Ref. 7) determined the power balance in nitrogen arcs at 1 atm. with currents of 40 to 100 amps in a 4.7mm diameter channel. Centerline temperatures ranged from 12,000°K to 13,700°K. The vacuum ultraviolet radiation transfer was calculated and found to be the dominant contributor to the radiation transfer within the column. Furthermore, energy transport via radiation in such arcs was found to be as important as that via conduction. Morris showed that Maecker's experimental data on the thermal conductivity of nitrogen could be lowered and brought into agreement with theory and Morris' work by inclusion of the previously ignored vacuum ultraviolet radiation transport.

Morris' conclusions do not contradict the conclusions in the paragraphs just above. His results show that the Maecker data need be corrected for the ultraviolet radiation only for T > 10,500°K, and that the correction increases nearly exponentially with temperature. Furthermore his results on the power transferred from the axis outward in an 100 amp. nitrogen arc, covering the temperature range 13,700 to 10,900°K, suggests that $\sigma E^2 >> u$ for the total radiation for temperatures near 11,000°K and below.

Thus Asinovsky (Ref. 3) and Morris (Ref. 7) seem to agree on the temperature above which radiation transfer becomes important in air and nitrogen arcs at 1 atm. and agree with Schreiber (Ref. 4) as to the relative amounts of the vacuum ultraviolet component. The results of Asinovsky and Schreiber suggest that the low temperature (T < 11,500°K), low pressure air arcs in this report would have $u << \sigma E^2$ even if u were to include the ultraviolet component. Therefore, although u(T) is subject to serious error from the incomplete radiation measurements, k(T) is not. At 30 atm. the situation may be different. The calibration or elimination of absorption along the optical path is expected to increase u(T) and reduce k(T). As measured u(T) was a few percent of σE^2 at 30 atm. Furthermore the radiation transport problem will have to be solved at 30 atm. before the comparison seen in Figure 21 can be taken seriously.

In concluding this report, some comments are made on possible future work.

The radiation measurements in this report should be completed by accounting for the absorption in the optical path at all wavelengths. Although the radiation per unit length escaping from the arc is of engineering interest in some applications, it is of value in determining the total emission coefficient or the thermal conductivity only if it can be related to a careful treatment of the radiation transport problem within the arc.

Since the temperature profiles at 30 atm. have been determined by only one method, the integrated line emission of the OI 844.6nm line, other lines or methods should be used for verification.

It appears that the apparatus will be useful at still higher pressures. The early air arc channels lasted about 5 minutes at 1 atm. It is now common to accumulate several hours of experimental time on each 1, 6 or 30 atm. air arc. The record at 30 atm. is now 37 hours for low current arcs (~15 amp.). Recently the apparatus has been run successfully many times at 100 atm. and several times at greater pressures up to 143 atm. The apparatus lifetimes at pressures in the range 100 to 143 atm. have been advanced to tens of minutes.

Preliminary results indicate that the OI 844.6nm line will still be useful in determining the temperature profiles at pressures greater than 30 atm., up to some limit. However, the increased absorption in the gas outside the arc will have to be calibrated, and the optical path improved to reduce the absorption to acceptable levels. Thus one can expect to be able to determine T(r) and hence $\sigma(T)$ at pressures higher than 30 atm. As already stated, the deduction of the emission coefficient and the thermal conductivity at higher pressures will depend upon successful radiation measurements and a solution of the radiation transport problem.

REFERENCES

1. W. E. Nicolet, et. al., "Analytical and Design Study for a High-Pressure, High-Enthalpy Constricted Arc Heater", Aerotherm/Acurex, Mountain View, CA, available as report AEDC-TR-75-47 (AD-A012551), Arnold Engineering Development Center, July 1975.

2. S. I. Andreev and T. V. Gavrilova, Teplofiz, Vys. Temp., 13, 176 (1975). (Engl. Trans., High Temperature, 13, 151 (1975).

3. E. I. Asinovsky, et. al,, Proc. of the IEEE 59, 592 (1971).

4. P. W. Schreiber, et. al., AIAA Journal 11, 815 (1973).

5. H. Maecker, Z. Physik 158, 392 (1960).

6. H. W. Emmons, Phys. Fluids 10, 1125 (1967).

7. J. C. Morris, et. al., Phys. Fluids 13, 608 (1970).

8. W. H. Venable, Jr. and J. B. Shumaker, Jr., J. Quant. Spectrosc. Radiat. Transfer 9, 1215 (1969).

9. U. H. Bauder and H. H. Maecker, Proc. of the IEEE 59, 588 (1971).

10. R. S. Devoto and D. Mukherjee, J Plasma Physics 9, 65 (1973).

11. H. R. Griem, Plasma Spectroscopy, McGraw-Hill, N.Y. (1964).

12. U. H. Bauder and E. D. Stephens, Rev. Sci. Instr. 43, 1341 (1972).

13. E. Shires, "Radial Temperature Profiles in an Air Arc", M.S.M.E. Thesis, Georgia Institute of Technology, Nov. 1974.

14. M. C. Wynn, "Investigation of Argon Plasma Properties", M.S.M.E. Thesis, Georgia Institute of Technology, Aug. 1975.

15. S. D. Thompson, "Radial Temperature Profiles in an RF Plasam over a Wide Range of Applied Magnetic Field Intensities; Theory and Experiment, Ph.D. Thesis", Georgia Institute of Technology, Feb. 1974.

16. A. S. Predvoditelev, et. al., "Tables of Thermodynamic Functions of Air for the Temperature Range 6,000-12,000°K and Pressure Range 0.001-1000 Atm." Infosearch Limited, London, distributed by Cleaver-Hume Press Ltd.

17. H. W. Drawin and P. Felenbok, Data for Plasmas in Local Thermodynamic Equilibrium, Gauthier-Villars, Paris, 1965.

18. National Standards Reference Data Series, National Bureau of Standards, No. 22, Vol. 2.

19. I. A. Sokolova, "Transport Coefficients of Air at Temperatures of from 3000 to 25,000°K at Pressures of 0.1, 1, 10, and 100 Atm., AD-779-809, FTD-HT-23-907-74, National Technical Information Service, Springfield, VA.

20. R. W. Liebermann, Westinghouse Research Laboratories, Pittsburg, Pa., 1976. (Private Communication).

21. Yos, J. M., "Transport Properties of Nitrogen, Hydrogen, Oxygen, and Air," RDS-TM-63-7, March 1963, AVCO/RAD, Wilmington, Mass.

22. Peng, T. C. and Pindroh, A. L., "An Improved Calculation of Gas Properties at High Temperatures: Air," Paper No. 1995-61, Fourth Biennial Gas Dynamics Symposium, American Rocket Society, Northwestern University, Evanston, Ill., August 23-25, 1961. (See comments in Ref. 1)